BMC Plant Biology

RESEARCH

Open Access

Amino acid metabolism pathways as key regulators of nitrogen distribution in tobacco: insights from transcriptome and WGCNA analyses

Shichen Li[1†], Waqar Ahmed[1†], Tao Jiang[1†], Dehai Yang[2], Linyuan Yang[1], Xiaodong Hu[1,3], Meiwei Zhao[1,4], Xiaoci Peng[1,3], Yingfen Yang[1,5], Wei Zhang[1], Mingmin Li[1] and Zhengxiong Zhao[1*]

Abstract

Background and aim Nitrogen (N) is crucial for plant growth and is distributed across various N morphologies within plant organs. However, the mechanisms controlling the distribution of these N morphologies are not fully understood. This study investigated key amino acid (AA) biosynthesis pathways regulating N distribution and their impact on plant physiology and growth.

Methods We examined N distribution in the leaves, stems, and roots of two tobacco cultivars (Hongda and K326) under different N treatments at 75, and 100 days after transplanting (DAT). Transcriptome analysis was performed at 75 and 100 DAT to explore N distribution and AA metabolism pathways. Weighted gene co-expression network analysis (WGCNA) identified pathways regulating N distribution, and the Mantel test assessed the impact of N treatments, growth stages, and cultivars on N distribution.

Results Statistically significant differences in N distribution were observed across environmental conditions, growth stages, cultivars, and plant organs ($p < 0.05$). WGCNA identified phenylalanine metabolism (ko00360), alanine, aspartate, and glutamate metabolism (ko00250), and glycine, serine, and threonine metabolism (ko00260) pathways regulating the distribution of $N_{in\text{-}SDS}$ (sodium dodecyl sulfate insoluble N), N_W (water soluble N), and N_S (sodium dodecyl sulfate soluble N), respectively. Increased N application promoted $N_{in\text{-}SDS}$ accumulation, while earlier growth stages and cultivar Hongda favored N_W distribution. N_S distribution was inhibited under high N conditions. Gene expression in these pathways correlated with N distribution, biomass, and N accumulation.

Conclusion This study elucidates the mechanisms regulating N distribution in tobacco, emphasizing the role of AA metabolism pathways. These findings are essential for improving N utilization and optimizing N management practices, ultimately enhancing crop productivity and supporting sustainable agricultural practices.

†Shichen Li, Waqar Ahmed and Tao Jiang contributed equally to this work.

*Correspondence:
Zhengxiong Zhao
zhaozx0801@163.com

Full list of author information is available at the end of the article

Keywords Tobacco (*Nicotiana tabacum L.*), nitrogen morphologies, amino acid pathways, WGCNA, Transcriptome analysis

Introduction

Nitrogen (N) is essential for crop growth and development and plays crucial roles in fundamental physiological processes such as photosynthesis, respiration, and protein synthesis [1, 2]. Within plants, N has various morphologies, each with distinct functions: water soluble N (N_W) for respiration, sodium dodecyl sulfate soluble N (N_S) for electron transfer and light absorption, non-protein N (N_{NP}) for storage, and sodium dodecyl sulfate insoluble N ($N_{in\text{-}SDS}$) for structural development [3–6]. Despite the known importance of N distribution, the mechanisms governing the distribution of different N morphologies and the implications of that distribution have yet to be elucidated. Factors such as environmental conditions, growth stages, plant organ types, and cultivar characteristics substantially influence N distribution patterns [5, 7]. For instance, increased N application has been associated with an altered distribution of N morphologies in various crops, impacting electron transfer, light capture (functions of N_s), and overall plant growth. Excess N can inhibit photosynthesis and negatively affect plant growth [5, 7]. Additionally, N fertilization influences traits such as effective tiller number in rice and vascular bundle structure in maize, potentially through modulation of the $N_{in\text{-}SDS}$ distribution, thereby influencing the N harvesting capacity as the plant matures [8, 9].

Diverse physiological activities at different stages lead to notable variations in N distribution. For example, primary N assimilation declines in senescent leaves, with released N remobilized into developing tissues such as new leaves and seeds, influencing physiological activities [10]. This process is closely related to N_{NP} degradation and its transformation into N_W, N_S, and $N_{in\text{-}SDS}$ for respiration, photosynthesis, and the development of new leaves [5, 11]. Furthermore, the N distribution varies markedly among plant organs, with roots and stems exhibiting higher N_{NP} and $N_{in\text{-}SDS}$ levels than leaves [2]. This variation underscores the importance of $N_{in\text{-}SDS}$ in roots for lignification, while higher levels of N_W and N_S in leaves contribute to photosynthesis, highlighting the association between N morphologies and organ function [2]. Genetic diversity among cultivars also contributes to variations in N distribution, with disparities in respiration (function of N_W) observed among wheat and sugar beet cultivars, ultimately contributing to differences in yield [12, 13]. Despite extensive research on the molecular mechanisms of N absorption and assimilation, relatively little attention has been given to elucidating the molecular mechanisms underlying N distribution within plants.

Amino acids (AA) play a central role in various physiological processes in plants, overlapping with the functions of different N morphologies. The AA biosynthetic pathway is crucial for N utilization, as it facilitates the synthesis of AAs from N [14]. Furthermore, AAs are involved in vital plant functions such as photosynthesis, respiration, and structural support [15]. For example, AAs activate photosynthesis, enhance light absorption, and serve as biological activators in respiration by providing energy and compensating for losses during respiration and degradation [16, 17]. Additionally, AAs are the building blocks of proteins, which are essential for maintaining the plant's structural integrity and supporting growth [18]. These overlapping functions highlight the critical role of AAs in N distribution. Like other N morphologies, AAs are influenced by factors such as N applications, growth stages, cultivar characteristics, and plant organs, all of which impact N morphologies distribution [18, 19].

Although N distribution across various plant organs has been extensively studied to improve N recovery and utilization, a substantial gap remains in research focused on the distribution of N morphologies in tobacco [20, 21]. To date, no studies have specifically explored the distribution of these N morphologies in tobacco. Moreover, even in other crops, comprehensive studies synthesizing the distribution patterns of different N morphologies across plant organs and exploring the mechanisms behind their transformation and allocation are scarce. Given the essential role of N in plant growth and development, there is an urgent need for research addressing both the distribution patterns and molecular mechanisms regulating these processes [22, 23].

We hypothesize that the AA synthesis pathway serves as a primary regulator of N allocation within plants, as AAs represent a key channel for N utilization, regulated by factors similar to those influencing N morphologies. Considering varying N application, cultivars, organs, and growth stages, distinct N distributions and genes in AA pathways are expected. By observing these distributions simultaneously, we aim to gain insights into the underlying mechanisms. Using weighted gene co-expression network analysis (WGCNA) based on transcriptome data, we will explore these mechanisms and analyze correlations among N morphologies across different factors, with a particular focus on AA pathways. Our objectives are as follows: (1) to explore how AA pathways regulate the transformation and distribution of N morphologies across plant organs (leaves, stems, and roots) at various growth stages; (2) to evaluate how cultivar

characteristics, N application rates, and growth stages influence N morphologies distribution; and (3) to identify key genes within AA pathways that modulate N distribution. The findings from this study will provide valuable insights into N metabolism and the role of AA pathways in N distribution. By enhancing our understanding of N use efficiency at the molecular level, this research will inform strategies to optimize N management, ultimately improving crop productivity and supporting sustainable agricultural practices in response to the growing global demand for N resources.

Materials and methods

Experimental site

The experiment was conducted in Yongping County, Dali Prefecture (25.6065°N, 100.2676°E), during the growing season from May to September in 2022. The site had an average annual precipitation of approximately 919.0 mm and an average temperature of 16.7 °C. The soil, classified as loam, had an organic matter content of 36.58 g/kg, with total nitrogen, phosphorus, and potassium levels of 1.95 g/kg, 0.82 g/kg, and 17.88 g/kg, respectively. The available nitrogen, phosphorus, and potassium concentrations were 233.10 mg/kg, 49.34 mg/kg, and 236.00 mg/kg, respectively. The climate and soil conditions at the site are suitable for the normal, high-quality growth of flue-cured tobacco, thus environmental factors, such as soil nutrient availability, were not controlled in this experiment and followed the natural conditions of the local area.

Experimental design and treatments

In this study, two flue-cured tobacco cultivars, Hongda and K326, were selected based on their distinct nitrogen use efficiencies. Hongda is recognized for its higher nitrogen use efficiency, making it particularly well-suited for nitrogen (N)-limited environments, while K326 has a higher N fertilizer requirement for optimal growth [2, 24]. Both cultivars, with distinct N use efficiencies, were individually transplanted into pots measuring 25 cm × 24 cm, each filled with 15 kg of loam soil. Each pot was irrigated with 1000 mL of water three times a week. The pots were arranged in rows, spaced 110 cm apart, with plants spaced 55 cm apart, resulting in a planting density of 16,500 plants per hectare [25]. Thirty plants were planted per treatment for each condition and experiment was repeated three times. N treatments were applied to the two tobacco cultivars, Hongda and K326, with three levels of N: 0 g (control), 4 g, and 8 g per plant. The treatments for Hongda were labeled H0 (no N), H4 (4 g N), and H8 (8 g N), while the treatments for K326 were labeled K0 (0 N), K4 (4 g N), and K8 (8 g N), respectively. The 0 g N treatments served as the control. The N concentrations of 4 g and 8 g were chosen to reflect typical local agricultural practices, with 8 g corresponding to the recommended application rate for K326 and 4 g for Hongda, based on their N uptake characteristics.

In all experimental pots, each plant received 2.5 g of pure phosphorus (P) and 10 g of pure potassium (K) fertilizer. Fertilizer was applied in two stages: 100% of N, 100% of P, and 80% of K were applied as base fertilizer at transplantation, followed by top-dressing with 20% of K 21 at days after transplantation (DAT). Management practices adhered to the National Standards of the Tobacco Industry in China [26], with no control over external environmental conditions, which were consistent with the local climate. In addition to the cultivars and N treatments, the study also investigated the effects of growth stages and plant organs.

Harvesting and sample analysis

Dry samples

After the tobacco plants were transplanted, samples were collected from the plants at 50, 75, and 100 DAT. After being harvested, the plants were divided into 3 distinct parts: roots, stems, and leaves by cutting the plant organs apart from each other. For each treatment, three tobacco plants per replicate were uprooted and destructively sampled at each growth stage. To remove excess soil, the sampled plants were thoroughly rinsed with running water, as described by Yang [27]. The fresh and dry weights of each plant part were recorded before and after curing. To ensure consistency, each plant part was initially dried at 105 °C for 30 min and then at 75 °C for 72 h as part of the curing process [28]. After being thoroughly crushed with a grinder, each dried plant part was sifted through a 2 mm mesh sieve before being crushed and digested with H_2SO_4-H_2O_2. Following the method outlined by Liu and fellows [5], the total N content of the digested plant material was determined through continuous flow analysis using an AA3 instrument (Seal Analytical Inc., Southampton, UK).

Fresh samples

Triplicate samples of middle leaves, middle stems, and root tips were collected from the plants directly at 75 and 100 DAT. The samples were rapidly frozen in liquid N. Each sample was then divided into two portions, with one portion allocated for RNA analysis and the other for N morphologies analysis.

Nitrogen morphologies in tobacco

The assessment of the N morphologies in the frozen tobacco plant samples followed the protocol outlined by Takashima [3]. 1 gram of each plant part, including leaves, roots, and stems, was frozen in liquid N. Subsequently, the frozen samples were homogenized with 1 mL of 100 mM sodium phosphate buffer consisting of 2

mM $MgCl_2$, 0.4 M d-sorbitol, 5 mM dithiothreitol, 5 mM iodoacetate, 10 mM NaCl, and 5 mM phenylmethylsulfonyl fluoride. The supernatant, containing water soluble N (N_W), was separated by centrifugation at 12,000 × g at 4 °C for 10 min. The residual samples were then dissolved in 1 mL of phosphate buffer containing 3% sodium dodecyl sulfate and heated at 90 °C for 5 min. Afterward, centrifugation at 5500 × g for 8 min was performed to collect the supernatant as sodium dodecyl sulfate soluble N (N_s). The insoluble residues, termed sodium dodecyl sulfate insoluble N ($N_{\text{in-SDS}}$), were purified with a 20 mL anhydrous ethanol wash and filtered through medium-speed filter paper. The supernatant was mixed with an equal volume of 20% trichloroacetic acid, filtered through quantitative filter paper, and thoroughly rinsed with 20 mL of anhydrous ethanol to denature the N compounds. Following natural air-drying, the residue on the quantitative filter paper underwent digestion using H_2SO_4-H_2O_2 following the methods of Luo and colleagus[29]. The N content of the digested solution was determined using continuous flow analysis (AA3; Seal Analytical Inc., Southampton, UK). The non-protein N (N_{NP}) content was calculated by subtracting the values of N_W, N_S, and $N_{\text{in-SDS}}$ from the total N content. The relative proportions of the various N morphologies to the total N content throughout the entire plant were determined using the subsequent equation.

$$Each\ N\ morphologies\ in\ leaves\ (\%) = \frac{The\ content\ of\ each\ N\ morphologies\ in\ leaves * Biomass\ of\ leaves}{The\ total\ nitrogen\ accumulation\ of\ whole\ plant\ (sum\ of\ leaves,\ and\ roots)} * 100\%$$

The results for the calculation of N morphologies in the stems and roots were similar to that for the leaves.

RNA extraction and transcriptome profiling

Total RNA was extracted from 108 frozen samples (3 N treatments × 2 DAT stages × 2 cultivars × 3 organs × 3 biological replicates per treatment) using TRIzol (Invitrogen Life Technologies, USA) according to the manufacturer's instructions. RNA degradation and contamination were monitored on 1% agarose gels [30, 31]. RNA purity was checked using a NanoPhotometer® spectrophotometer (IMPLEN, CA, USA). The RNA concentration was measured using a Qubit® RNA Assay Kit in a Qubit® 2.0 Fluorometer (Life Technologies, CA, USA). RNA integrity was assessed using the RNA Nano 6000 Assay Kit for the Bioanalyzer 2100 system (Agilent Technologies, CA, USA).

Library Preparation

A total of 1 μg of RNA per sample was used as input material for the RNA sample preparations. Sequencing libraries were generated using the NEBNext® UltraTM RNALibrary Prep Kit for Illumina® (NEB, USA) following the manufacturer's recommendations. First-strand cDNA was synthesized using a random hexamer primer and M-MuLV reverse transcriptase (RNase H-). Second-strand cDNA synthesis was subsequently performed using DNA Polymerase I and RNase H [32, 33]. To preferentially select cDNA fragments 250–300 bp in length, the library fragments were purified with the AMPure XP system (Beckman Coulter, Beverly, USA) [32]. Then, 3 μl of USER Enzyme (NEB, USA) was incubated with size-selected, adaptor-ligated cDNA at 37 °C for 15 min, followed by 5 min at 95 °C before PCR. Then, PCR was performed with Phusion High-Fidelity DNA polymerase, universal PCR primers, and Index (X) Primer. Finally, the PCR products were purified (AMPure XP system), and library quality was assessed on an Agilent Bioanalyzer 2100 system [34].

Data quality control, processing, and functional annotation analysis

Fastp v0.19.4 was used to filter the original data to remove reads with adapters, reads with N content > 10% of the total bases, and sequencing reads with low-quality (Q ≤ 20) bases contained in the reads that exceeded 50% of the bases to produce clean reads [35]. Transcriptome assembly was performed using Trinity (v2.11.0), and Corset was used to regroup relevant transcripts into 'gene' clusters (https://github.com/trinityrnaseq/trinityrnaseq) [36]. TransDecoder (https://github.com/TransDecoder/TransDecoder/wiki) was used to identify candidate coding regions within transcript sequences generated by de novo RNA-Seq transcript assembly using Trinity [35]. Gene function was annotated using Diamond or HMMER with the following databases: Nr, Swiss-Prot, Trembl, Kyoto Encyclopedia of Genes and Genomes (KEGG) [37], and Gene Ontology (GO) [38]. Gene expression levels were estimated with RNA-seq by expectation maximization, and then the fragments per kilobase of transcript per million mapped reads (FPKM) of each gene were calculated based on the gene length. DESeq2 v1.22.1 was used to analyze the differentially expressed genes between the two groups, and a difference analysis was performed using edgeR [36]. The p value was corrected using the Benjamini and Hochberg method. A corrected p value < 0.05 and |log2foldchange| > 1 were used as the thresholds of statistical significance for analyzing differences in expression [39]. The enrichment analysis was performed based on the hypergeometric test [40]. For the KEGG analysis, the hypergeometric distribution test was performed according to the unit of the pathway, and for

the GO analysis, it was performed according to GO terms [32]. Missing data in the transcriptomic analysis were handled using multiple imputation to replace the missing values. This approach ensures a more robust dataset by considering the uncertainty introduced by missing data, allowing for more reliable downstream analysis and statistical inference [41, 42].

Validation of RNA-seq data by RT-qPCR

Total RNA was isolated utilizing the KKFast Plant RNA-pure Kit (ZP405K-2, Zoman Biotech, Beijing, China). cDNA was synthesized using a SuperMix cDNA synthesis kit (AT311-03, Transgene Biotech, Beijing, China). RT-qPCR was performed using Universal SYBR qPCR Mastermix (Q712-02, Vazyme, China) under the following conditions: initial denaturation at 95 °C for 30 s, followed by 40 cycles of denaturation at 95 °C for 10 s and annealing/extension at 58 °C for 30 s. The relative gene expression was determined utilizing the $2^{-\Delta\Delta C}$t method [43] and all experiments were performed in triplicate. The sequences of primers used in this study are listed in Table S1.

Data analysis

The statistical analysis was performed using analysis of variance (ANOVA) with the F-test in SPSS Version 23.0, where statistical significance was determined based on the F-value and its associated $p < 0.05$ [44]. Waterfall plots for biomass and N accumulation were generated using OriginLab Version 2022. Sector figures to describe N distribution were generated using the "ggplot2" package in R. Before conducting the transcriptome data analysis, the data were normalized using the DESeq2 package in R, and the scale function was applied to standardize the data by rows [45]. Heatmaps were created using the "pheatmap" package in R. Constrained principal coordinates analysis (CPCoA) charts to visualize the differences among the different treatments were generated using the "ggplot2" package in R [45]. Weighted gene co-expression network analysis (WGCNA) was performed using MetWare Cloud (https://cloud.metware.cn) to construct co-expression networks. No gene filtering was applied before the analysis. Modules were merged with a minimum height of 0.2 for pruning, and a minimum of 400 genes were required for each module. An R^2 value of 0.85 was used as the threshold for selecting the genes involved in co-expression [46]. The chord diagram figure was created using the "circlize" package in R. Network charts were created using Cytoscape 3.10.1 [47]. Pathway charts were generated using Office Publisher 365. Mantel test charts were generated using the "vegan" and "ggcor" packages [48], with the Mantel test conducted using the mantel test function, applying Bray-Curtis dissimilarity for species data and Euclidean distance for environmental data. The statistical significance was determined using p values, categorized as: $p < 0.001$, $p < 0.01$, $p < 0.05$ (statistical significance) and $p \geq 0.05$ (not statistical significance). The figures were refined and compiled using Adobe Illustrator Version 2019.

Table 1 ANOVA test (F-test, $p < 0.05$) conducted on biomass and nitrogen accumulation across different organs at various stages, under different treatments, and in different cultivars

Index	Biomass		Nitrogen	
	F	*p*	F	*p*
Days after transplanting	31.885	0.001	419.375	0.001
Treatments	20.394	0.001	995.956	0.001
Cultivars	13.277	0.001	481.799	0.001
Organs	181.196	0.001	7246.603	0.001

Here, F-values and *p*-values were derived from the F test. Statistical significance was defined as $p < 0.05$

Results

The accumulation of nitrogen and biomass

All results were derived from three independent biological replicates, with plants grown in separate pots under controlled conditions to minimize variability. One-way ANOVA (F-test) revealed statistically significant differences in biomass and nitrogen (N) accumulation across treatments, cultivars, growth stages, and organs (Table 1). Specifically, the effects of treatments ($F = 20.394$, $p < 0.001$), cultivars ($F = 13.277$, $p < 0.001$), growth stages ($F = 31.885$, $p < 0.001$), and organs ($F = 181.196$, $p < 0.001$) were all statistically significant for biomass accumulation (Table 1). Similarly, Treatments statistically significantly influenced N accumulation ($F = 995.956$, $p < 0.001$), cultivars ($F = 481.799$, $p < 0.001$), growth stages ($F = 419.375$, $p < 0.001$), and organs ($F = 7246.603$, $p < 0.001$) (Table 1). To elucidate the N distribution mechanism, our initial focus was on determining biomass and N accumulation across various stages. Differences in biomass accumulation among the various treatments were assessed for statistical significance in relation to quantity of days after transplanting (DAT), plant organs, and cultivars (Fig. 1). Notably, compared to the non-N application treatments, among the different treatments, the application of 4 g and 8 g of pure N resulted in a 52.07% and 76.14% increase in biomass, respectively. As the stages progressed, biomass accumulation increased by 95.13% from 50 DAT to 75 DAT and by 25.41% from 75 DAT to 100 DAT. The analysis of the different tobacco organs revealed a greater biomass concentration in the leaves, which accounted for 54.24% of the total plant biomass, while stems and roots accounted for 40.23% and 5.54%, respectively. The Hongda cultivar exhibited 1.29 times greater biomass accumulation than did the K326 cultivar.

Furthermore, a statistically significant difference in N accumulation was detected (Fig. 2). Compared with the

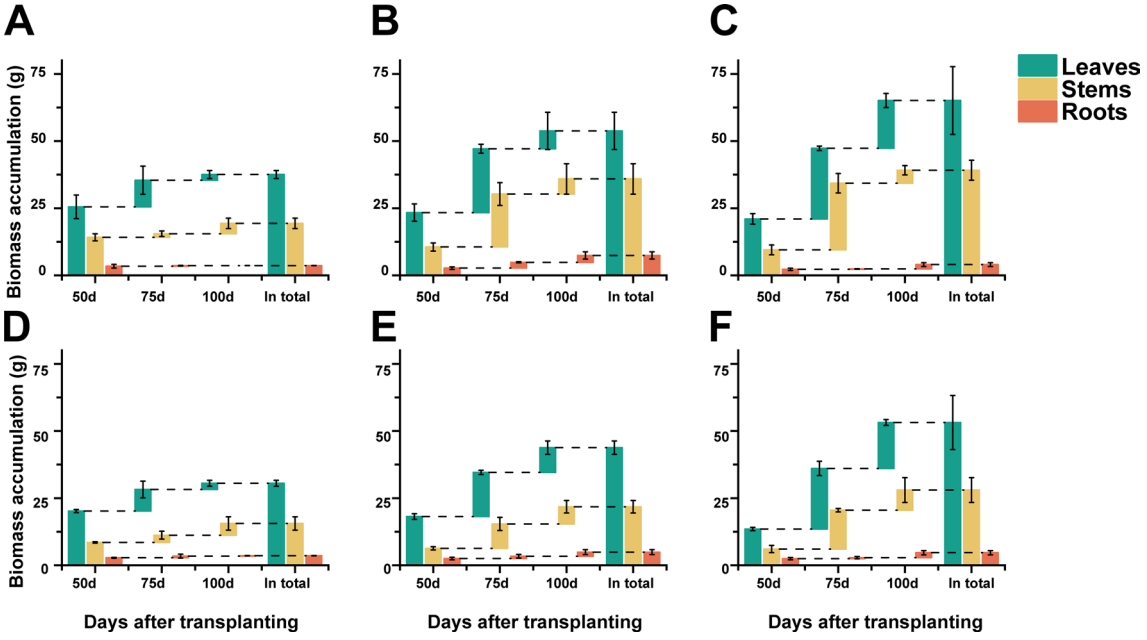

Fig. 1 Waterfall chart illustrating the accumulation of biomass in different plant organs (leaves, stems, and roots) at various growth stages. The chart shows the progression of biomass accumulation across treatments and cultivars, highlighting the differences in biomass allocation at each growth stage (see Table 1 for F-values and *p* values, $p < 0.05$). Panels **A** to **F** depict nitrogen accumulation in the Hongda (H0, H4, H8) and K326 (K0, K4, K8) cultivars under 0 g, 4 g, and 8 g pure nitrogen conditions, respectively. Here, H0, H4, and H8 represent the Hongda cultivar under 0 g, 4 g, and 8 g pure nitrogen conditions, respectively, while K0, K4, and K8 represent the K326 cultivar under each nitrogen condition

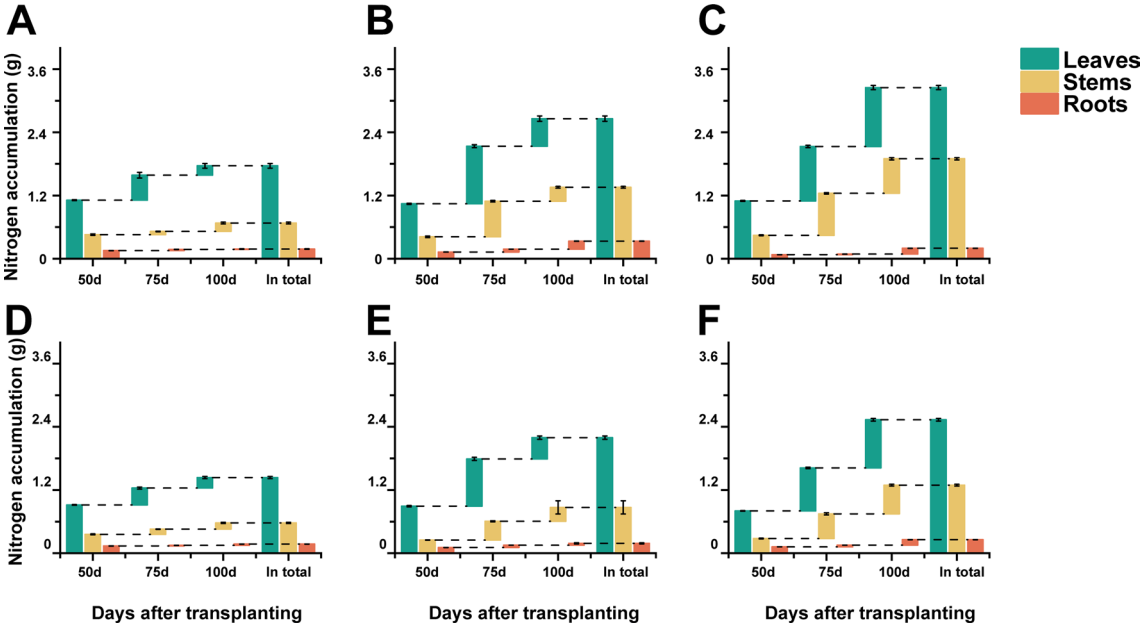

Fig. 2 Waterfall chart illustrating the accumulation of nitrogen in different plant organs (leaves, stems, and roots) at various growth stages. The chart shows the progression of nitrogen accumulation across treatments and cultivars, highlighting the differences in nitrogen allocation at each growth stage(see Table 1 for F-values and *p* values). Panels **A** to **F** depict nitrogen accumulation in the Hongda (H0, H4, H8) and K326 (K0, K4, K8) cultivars under 0 g, 4 g, and 8 g pure nitrogen conditions, respectively. Here, H0, H4, and H8 represent the Hongda cultivar under 0 g, 4 g, and 8 g pure nitrogen conditions, respectively, while K0, K4, and K8 represent the K326 cultivar under each nitrogen condition

non N treatments, the application of 4 g and 8 g of pure N resulted in a 58.06% and 96.12% increase in N, respectively. Similar to biomass accumulation, N accumulation increased with DAT, with an 82.75% from 50 DAT to 75 DAT and a 35.96% from 75 DAT to 100 DAT. N enrichment was more pronounced in leaves, which accounted for 63.37% of the total plant N, while stems and roots accounted for 30.53% and 6.10% of N, respectively. Additionally, between the two cultivars, Hongda accumulated 29.42% more N than did the K326 cultivar.

Nitrogen distribution across various plant morphologies

All results were based on three biological replicates, with samples processed in parallel to reduce technical variability. Statistically significant differences in N distribution were observed across treatments, cultivars, and organs (Table 2). Specifically, the distribution of sodium dodecyl sulfate insoluble N ($N_{\text{in-SDS}}$) was statistically significantly affected by treatments (F = 49.551, $p < 0.001$), cultivars (F = 380.823, $p < 0.001$), and organs (F = 6062.689, $p < 0.001$) (Table 2). Similarly, the distributions of water-soluble N (*N*w) and sodium dodecyl sulfate soluble N (N_S) showed strong effects of treatments (F = 66.611 and 15.158, $p < 0.001$), cultivars (F = 326.590 and 194.212, $p < 0.001$), and organs (F = 1767.426 and 2568.270, $p < 0.001$) (Table 2). However, no statistically significant differences in N_S distribution were observed across growth stages (F = 0.644, $p = 0.527$; Table 2).

Furthermore, we aimed to determine N distribution in plants. The N distribution statistically significantly differed among the different treatments, after transplanting, and between the Hongda and K326 cultivars (Fig. 3). In leaves, a decrease in N application led to an increase in non-protein N (N_{NP}) distribution, while $N_{\text{in-SDS}}$ initially increased and then decreased with increased N application. Conversely, the patterns of N_W and N_S showed the opposite trend to that of $N_{\text{in-SDS}}$. In stems, greater N application resulted in greater distributions of N_W and N_S. However, in roots, increased N application notably decreased the ratio of various N morphologies.

Between 75 and 100 DAT, the percentages of N_S and N_{NP} in the leaves decreased from 17.62 to 15.38% and from 11.83 to 7.33%, respectively. Among the different organs, in leaves, more N was distributed in the morphologies of $N_{\text{in-SDS}}$ and N_W, which constituted 30.03% and 29.82% of the total N accumulation in the leaves, respectively. In stems, more N was distributed in the morphologies of N_{NP} and N_W, accounting for 42.56% and 31.56% of the total stem N accumulation, respectively. In roots, more N was distributed in the morphologies of N_W and $N_{\text{in-SDS}}$, comprising 39.00% and 27.98% of the total N accumulation, respectively. Regarding the differences between the Hongda and K326 cultivars, in Hongda, more N was distributed as N_W in stems and leaves, with levels 6.86% and 3.85% greater than those in K326, respectively. Conversely, in K326, more N was distributed in the morphologies of N_{NP} in stems and in the morphologies of $N_{\text{in-SDS}}$ in leaves, with levels 8.44% and 6.80% greater than those in Hongda (Figure 3).

Transcriptome analysis

Transcriptome sequencing was performed on the leaves, stems, and roots of the two tobacco cultivars harvested at 75 and 100 DAT under 0 g, 4 g, and 8 g pure N treatments (Tables S2–S7) using the Illumina HiSeq platform. In amalgamating the data from leaves, stems and roots, the number of clean reads ranged from 40.43 million to 60.08 million, averaging 45.98 million. The effective base counts varied between 6.07 and 9.01 GB, with the Q20 content averaging 97.19% and the Q30 content averaging 92.12%. Quality control assessments consistently indicated mismatch rates below 0.03% for the datasets, confirming the suitability of the transcriptome data for subsequent analyses. The constrained principal coordinates analysis (CPCoA) analysis revealed that gene expression substantially varied among different N conditions, organs, stages, and cultivars (Fig. 4). Under the same N conditions, the gene expression profiles of the three replicates exhibited high similarity.

Functional enrichment analysis of differentially expressed genes in KEGG pathways

Kyoto Encyclopedia of Genes and Genomes (KEGG) enrichment analysis revealed organ-specific N modulation of metabolic pathways. In leaves (Fig. 5A), N application differentially regulated amino acid (AA) biosynthesis

Table 2 ANOVA test (F-test, $p < 0.05$) conducted on different morphologies nitrogen across different organs at various stages, under different treatments, and in different cultivars

Index	$N_{\text{in-SDS}}$		N_W		N_S		N_{NP}	
	F	*p*	F	*p*	F	*p*	F	*p*
Days after transplanting	49.275	0.001	13.044	0.001	0.644	0.527	333.406	0.001
Treatments	49.551	0.001	66.611	0.001	15.158	0.001	25.454	0.001
Cultivars	380.823	0.001	326.590	0.001	194.212	0.001	28.036	0.001
Organs	6062.689	0.001	1767.426	0.001	2568.270	0.001	96.229	0.001

Here, N presents nitrogen, $N_{\text{in-SDS}}$ represents sodium dodecyl sulfate insoluble nitrogen, N_S represents sodium dodecyl sulfate soluble nitrogen, N_W represents water soluble nitrogen and N_{NP} present non-protein nitrogen

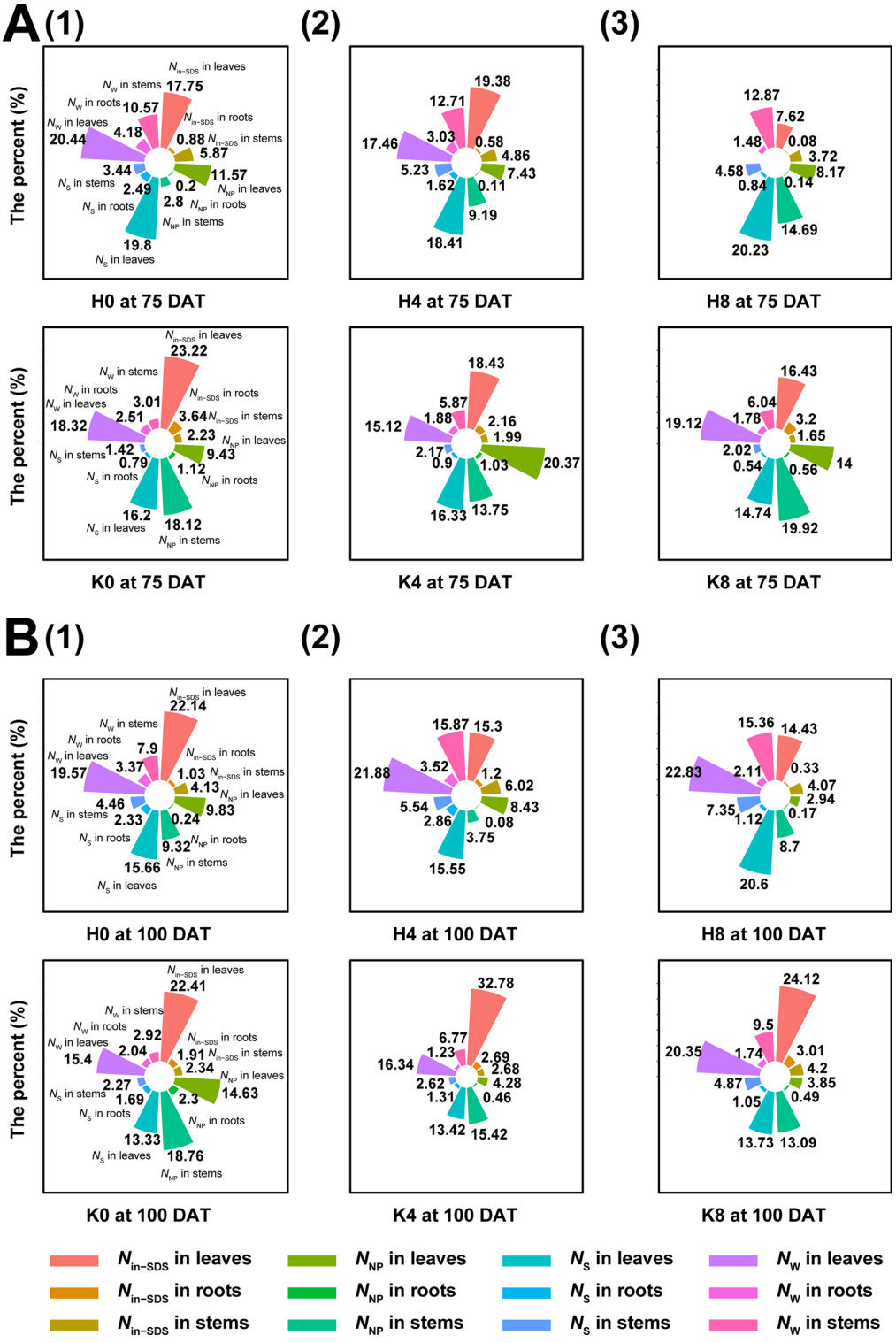

Fig. 3 Sector figures illustrating the distribution of various nitrogen (N) morphologies in different plant organs. Each sector represents the relative distribution of these nitrogen forms in leaves, stems, and roots, offering insight into how nitrogen is allocated within the plant under varying conditions (see Table 2 for F-values and *p* values). Panels A and B represent the nitrogen distribution at 75 days and 100 days after transplanting, respectively. Figures A (1) to A (6) and B (1) to B (6) represent the distributions under different treatments: H0, H4, H8, K0, K4, and K8, respectively. Here, H0, H4, and H8 denote the Hongda cultivar under 0 g, 4 g, and 8 g pure nitrogen conditions, respectively, while K0, K4, and K8 represent the K326 cultivar under each nitrogen treatment. Here, $N_{in\text{-}SDS}$ represents sodium dodecyl sulfate insoluble nitrogen, N_S represents sodium dodecyl sulfate soluble nitrogen, N_W represents water soluble nitrogen and N_{NP} present non-protein nitrogen

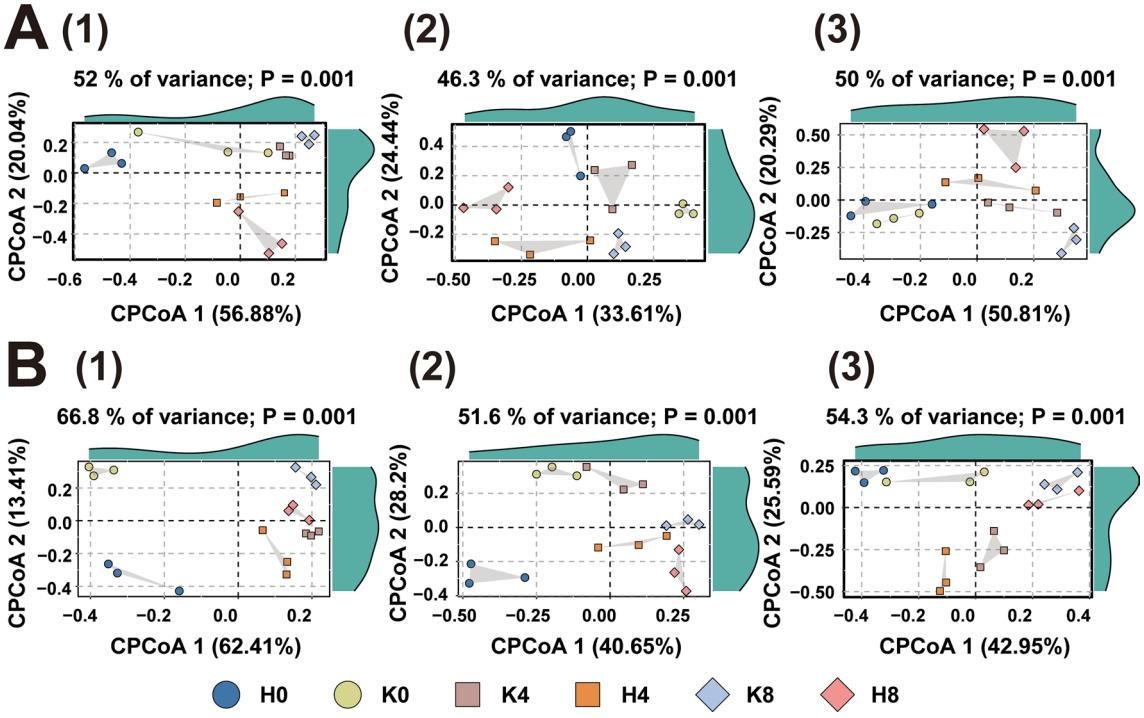

Fig. 4 Constrained principal coordinates analysis (CPCoA) analysis revealing differences among different nitrogen conditions, organs, stages, and cultivars, as well as similarities within the same condition across three replications. Panels **A** (1) to (3) illustrate the expression patterns of each replication in leaves, stems, and roots, respectively, at 75 days after transplanting (DAT). Panels **B** (1) to (3) show the expression patterns of each replication in leaves, stems, and roots at 100 DAT. Here, H0, H4, and H8 denote the Hongda cultivar under 0 g, 4 g, and 8 g pure nitrogen conditions, respectively, while K0, K4, and K8 represent the K326 cultivar under each nitrogen condition

(ko01230), glutathione metabolism (ko00480), and alanine, aspartate, and glutamate metabolism (ko00250), with the most pronounced transcriptional shifts occurring in late-stage treatments. Cultivar-specific responses were particularly evident under low N, where Hongda exhibited greater differential expression than K326 at 75 DAT. Stems (Fig. 5B) showed N-dependent reprogramming of cysteine and methionine metabolism (ko00270) and carbon metabolism (ko01200), especially under prolonged N limitation, while roots (Fig. 5C) prioritized phenylpropanoid biosynthesis (ko00940) and amino sugar metabolism (ko00520) in response to high-N conditions. Cross-organ comparisons (Fig. 5D) further demonstrated systemic coordination: glutathione metabolism and AA biosynthesis were consistently regulated across all organs at 75–100 DAT, with late-stage treatments (100 DAT) driving stronger divergence than earlier phases. Notably, Hongda displayed enhanced metabolic plasticity compared to K326, particularly under low-N stress. These findings collectively establish N availability as a central orchestrator of spatiotemporal metabolic adaptation, fine-tuning organ-specific pathways to balance growth and stress resilience.

Our findings demonstrate that N application regulates the expression of key AA-related pathways, including Biosynthesis of AA, Cysteine and methionine metabolism, Glutathione metabolism, and Amino sugar and nucleotide sugar metabolism. These pathways showed differential gene expression patterns across N treatments, with particularly pronounced changes. Notably, across all two cultivars, three organs, and two growth stages, these pathways exhibited consistent and substantial changes under different N treatments, indicating that N application induces similar alterations in these pathways regardless of the cultivars, organs, or growth stages.

Functional enrichment analysis of differentially expressed genes in GO pathways

Gene Ontology (GO) enrichment analysis revealed N-dependent regulation of metabolic and transport functions across organs. In leaves (Fig. 6A), treatments with contrasting N availability showed pronounced differences in glucosyltransferase activity (GO:0008194) and photosystem components (GO:0009521)—processes critical for nitrogen-dependent carbon fixation. Similarly, stems (Fig. 6B) exhibited nitrogen-responsive variations in plasma membrane anchoring (GO:0046658) and photosystem I/II activity, particularly under prolonged N limitation. Roots (Fig. 6C) displayed N-modulated shifts in UDP-glucosyltransferase activity (GO:0035251) and polysaccharide catabolism (GO:0000272), with marked differential expression in high-N treatments. Cross-organ

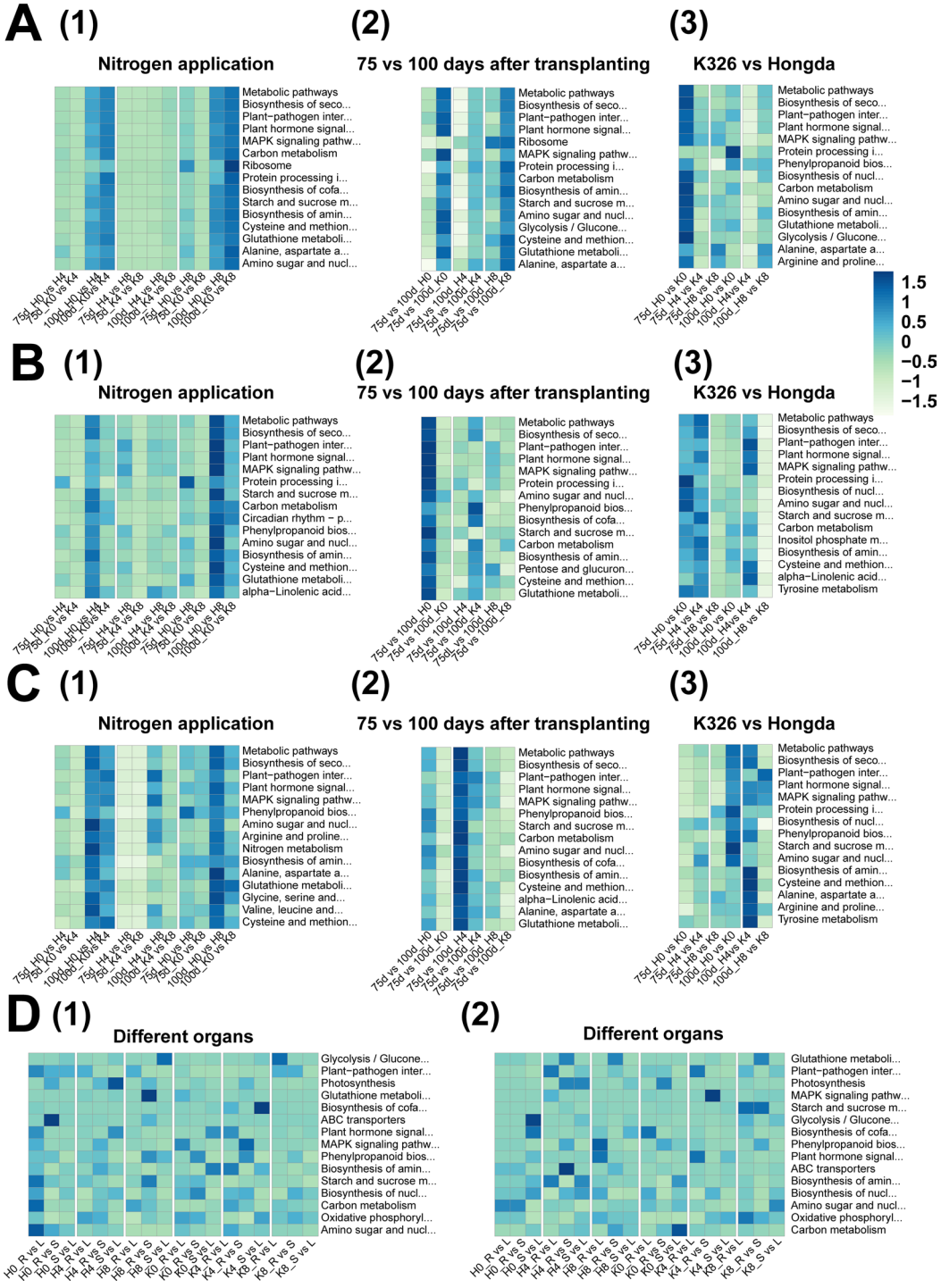

Fig. 5 Heatmap depicting the results of enrichment analysis for differential gene expression in Kyoto Encyclopedia of Genes and Genomes (KEGG) pathways across various comparisons. The analysis compares the effects of different nitrogen (N) application rates, cultivars, growth stages, and plant organs on gene expression. Panels (**A**) to (**C**) display differences observed in leaves, stems, and roots, respectively, while Panel (**D**) illustrates variations among different organs. Within Panels A to C, subpanels (1) to (3) correspond to differences among different nitrogen treatments, stages, and cultivars, respectively. Panel D includes subpanels (1) and (2), indicating variances at 75 and 100 days after transplantation, respectively. Here, H0, H4, and H8 denote the Hongda cultivar under 0 g, 4 g, and 8 g pure nitrogen conditions, respectively, while K0, K4, and K8 represent the K326 cultivar under each nitrogen condition

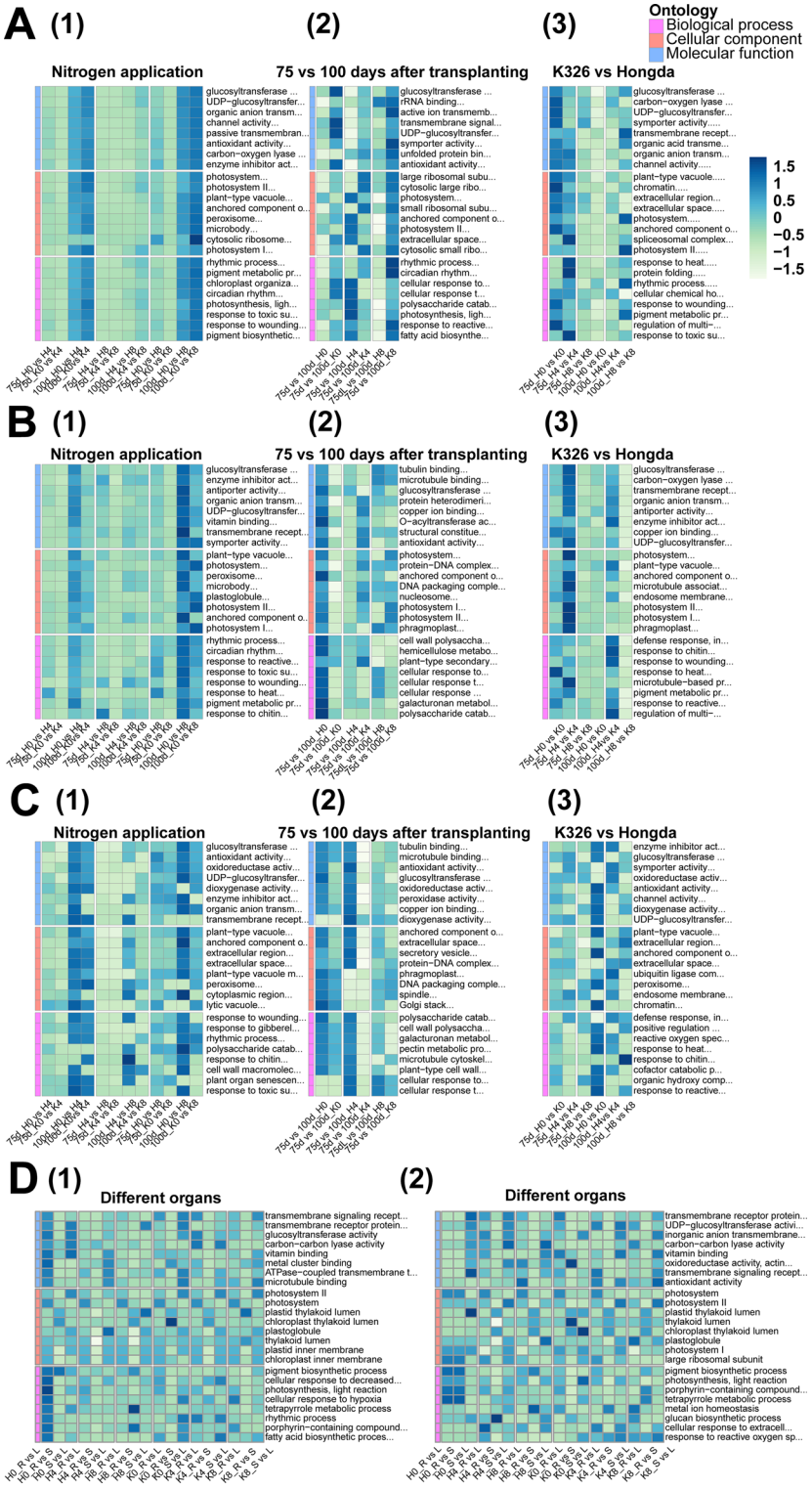

Fig. 6 Heatmap depicting the results of enrichment analysis for differential gene expression in Gene Ontology (GO) pathways across various comparisons. The analysis compares the effects of different nitrogen (N) application rates, cultivars, growth stages, and plant organs on gene expression. Panels (**A**) to (**C**) display differences observed in leaves, stems, and roots, respectively, while Panel (**D**) illustrates variations among different organs. Within Panels A to C, subpanels (1) to (3) correspond to differences among different nitrogen conditions, stages, and cultivars, respectively. Panel D includes subpanels (1) and (2), indicating variances at 75 and 100 days after transplantation, respectively. Here, H0, H4, and H8 denote the Hongda cultivar under 0 g, 4 g, and 8 g pure nitrogen conditions, respectively, while K0, K4, and K8 represent the K326 cultivar under each nitrogen condition

comparisons (Fig. 6D) further highlighted N-linked adaptations: transmembrane receptor kinases (GO:0019199) and inorganic anion transporters (GO:0015103) were differentially regulated, particularly at 75–100 DAT under N-varying conditions.

We further identified notable variations in specific GO categories: glucosyltransferase activity (GO:0046527), UDP-glycosyltransferase activity, and organic anion transport in the plant-type vacuole (GO:0015698). These observations reveal N-dependent modulation of metabolic functions spanning cell wall biogenesis, secondary metabolite modification, and nutrient partitioning under contrasting cultivation conditions across the different cultivars, organs, or growth stages.

WGCNA between DEGs and nitrogen distribution

To identify genes associated with N distribution in plants, we utilized Weighted Gene Co-expression Network Analysis (WGCNA) to define key modules, construct a gene co-expression network, and pinpoint hub genes. This analysis was conducted using transcriptome data from 108 samples, incorporating N morphologies at 75 and 100 DAT, as well as biomass and N increase between 50 and 75 DAT and 75–100 DAT. The clustering results from the dendrogram (Fig. 7A) revealed 16 distinct modules, each representing a cluster of highly correlated genes.

Among these 16 modules, three were strongly correlated with N-related traits: the brown module with $N_{\text{in-SDS}}$, the green module with *N*w, and the magenta module with N_S. Each of these modules exhibited a statistically significant positive correlation with N and biomass increment (Fig. 7B). Notably, the brown module showed a correlation coefficient of 0.84 with $N_{\text{in-SDS}}$, the green module had a 0.83 correlation with *N*w, and the magenta module exhibited a 0.92 correlation with N_S ($p < 0.05$).

To validate the reliability of the WGCNA modules, we integrated two key statistical approaches. First, the strong positive correlation between module membership and gene statistical significance confirmed that hub genes in core modules regulate the target phenotype (Fig. 7C, $p < 0.05$). Second, the gene co-expression network heatmap showed high topological overlap measure values within modules, indicating consistent co-expression, while low inter-module topological overlap measure values validated module independence (Fig. 7D). These results demonstrate the biological relevance and structural coherence of the WGCNA modules, linking them to phenotypic traits and ensuring functional unity for further mechanistic study.

Further KEGG pathway analysis (Fig. 7E1) revealed that the brown module is associated with phenylalanine metabolism (ko00360), the green module with alanine, aspartate, and glutamate metabolism (ko00250), and the magenta module with glycine, serine, and threonine metabolism (ko00260). These pathways showed distinct enrichment patterns, highlighting their unique roles in N metabolism. The GO analysis (Fig. 7E2) also identified substantial enrichment in genes involved in the biosynthesis, regulation, and transport of organic N compounds, underscoring their relevance in N distribution regulation.

The gene co-expression network was further analyzed using Cytoscape, identifying hub genes within the brown, green, and magenta modules (Fig. 7F). Key hub genes such as *LOC107788402* and *LOC107762576* in the brown module (Fig. 7F1), *LOC107802035* and *LOC107766022* in the green module (Fig. 7F2), and *LOC107803058* and *LOC107765918* in the magenta module (Fig. 7F3) were found to play critical roles in regulating N distribution (Table 3).

Functional pathway analysis from WGCNA modules

To further understand the molecular mechanisms regulating N distribution, we analyzed the relationships between the pathways of each hub gene in the brown, green, and magenta modules and the distribution of different N morphologies. To validate these observations, quantitative real-time polymerase chain reaction (RT-qPCR) was performed. RT-qPCR analysis was conducted on the examined genes, further emphasizing their relevance through the highest number of linked genes they displayed. The RT-qPCR results confirmed consistent expression patterns among the different treatments, growth stages, organs, and cultivars, as illustrated in Fig. 8, and the RT-qPCR results are shown in Table S8-S10.

The functional annotation of key modules revealed distinct AA metabolic pathways driving N distribution across morphologies. In the brown module related to phenylalanine metabolism (Fig. 8A), key processes include the interconversion of phenethylamine and phenylacetaldehyde, L-phenylalanine and phenylpyruvate, as well as phenylpyruvate to 2-hydroxy-3-phenylpropenoate, and the conversion of 2-phenylacetamide to phenylacetic acid. In the green module of alanine, aspartate, and glutamate metabolism (Fig. 8B), genes are involved in processes such as the interconversion of L-aspartate and L-asparagine, adenylosuccinate transformation to fumarate, L-glutamate to L-glutamine, and L-glutamine to D-glucosamine phosphate. In the magenta module of glycine, serine, and threonine metabolism (Fig. 8C), key processes include the interconversion of hydroxypyruvate and D-glycerate, L-serine and glycine, and the transformation of choline to betaine aldehyde and subsequently to betaine.

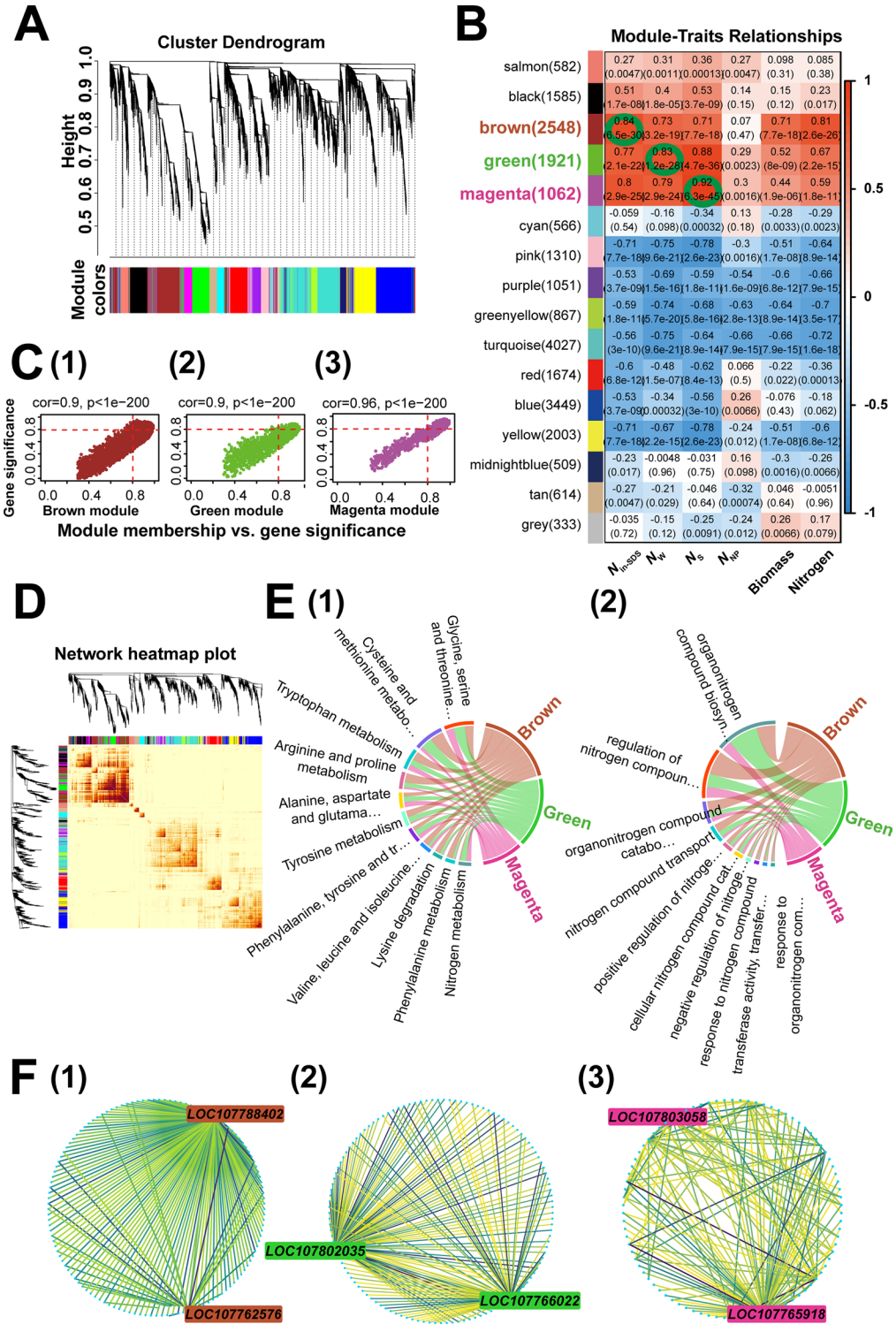

Fig. 7 WGCNA (Weighted Gene Co-expression Network Analysis) was used to explore the relationship between the ratio of each nitrogen morphologies and gene expression. Panel (**A**) presents the cluster dendrogram results, while Panel (**B**) depicts module-trait relationships. Panel (**C**) shows scatter plots illustrating the significance between module membership and genes, with subpanels (1) to (3) detailing the results of the selected brown, green, and magenta modules, respectively.Panel (**D**) displays a network heatmap illustrating the connectivity strength between nodes. Panel (**E**) features chord diagram figures revealing the enrichment analysis results of differential gene expression in brown, green, and magenta modules, with subpanels (1) to (2) presenting the results of the Kyoto Encyclopedia of Genes and Genomes (KEGG) and Gene Ontology (GO) analyses, respectively. Finally, Panel (**F**) presents the results of network analysis, with subpanels (1) to (3) delineating the results of the brown, green, and magenta modules, respectively. Here, $N_{\text{in-SDS}}$ represents sodium dodecyl sulfate insoluble nitrogen, N_S represents sodium dodecyl sulfate soluble nitrogen, N_W represents water soluble nitrogen and N_{NP} present non-protein nitrogen

Table 3 Functional prediction of hub genes

Module	Hub gene ID	KEGG Pathway	Gene Function
Brown	LOC107788402	Phenylalanine metabolism	K07253 phenylpyruvate tautomerase [EC:5.3.2.1]| (RefSeq) macrophage migration inhibitory factor homolog (A)
	LOC107762576	Phenylalanine metabolism	K07253 phenylpyruvate tautomerase [EC:5.3.2.1]| (RefSeq) macrophage migration inhibitory factor homolog (A)
Green	LOC107802035	Alanine, aspartate and glutamate metabolism	K01915 glutamine synthetase [EC:6.3.1.2]| (RefSeq) nepGS; glutamine synthetase, chloroplastic-like (A)
	LOC107766022	Alanine, aspartate and glutamate metabolism	K01915 glutamine synthetase [EC:6.3.1.2]| (RefSeq) nepGS; glutamine synthetase, chloroplastic (A)
Magenta	LOC107803058	Glycine, serine and threonine metabolism	K14272 glutamate–glyoxylate aminotransferase [EC:2.6.1.4 2.6.1.2 2.6.1.44]| (RefSeq) glutamate–glyoxylate aminotransferase 2-like (A)
	LOC107765918	Glycine, serine and threonine metabolism	K15893 glycerate dehydrogenase [EC:1.1.1.29]| (RefSeq) glycerate dehydrogenase (A)

Here, KEGG present the Kyoto Encyclopedia of Genes and Genomes

Regulation of factors influencing gene expression in each amino acid pathway

Furthermore, Mantel tests were conducted to assess the relationships between gene expression patterns and N applications, growth stages, organ types, and cultivars. These tests are important as they help determine the strength and significance of correlations between multiple variables, allowing us to better understand the factors influencing gene expression. Specifically, the effects of N applications, growth stages, organ types, and cultivars on gene expression were assessed by assigning the following values: N application rates were based on the actual N doses applied (0, 4, 8 g N per plant), reflecting the impact of N supply on gene expression; 75 DAT was designated as 1, and 100 DAT as 2, representing the progression of gene expression patterns as the plant develops; leaves were assigned as 1, stems as 2, and roots as 3, based on increased lignification, which is closely related to N distribution within the plant and reflects gene expression variation among organs; and the Hongda cultivar was assigned as 1 and K326 as 2, to differentiate the cultivars with distinct N use efficiencies and analyze their gene expression patterns. The significance of the Mantel test was determined based on a p value threshold, with the following classifications: $p < 0.001$ *()*, $0.001 \le p < 0.01$ *()*, $0.01 \le p < 0.05$ *()*, and $p \ge 0.05$ (not statistical significance).

The Mantel test revealed statistically significant correlations between gene expression and N applications, growth stages, organs, and cultivars (all $p < 0.05$). In the phenylalanine metabolism pathway (Fig. 9A), N application statistically significantly decreased the expression of *LOC107759078* and *novel.18,015* ($p < 0.05$), while increasing other genes ($p < 0.05$), with cultivar Hongda exhibiting higher expression of *LOC107759078*, *LOC107764910*, and *LOC107819268* compared to K326 ($p < 0.05$). Gene expression varied statistically significantly across growth stages, showing elevated levels at 75 DAT for *LOC107762576* and *LOC107788402* ($p < 0.05$), and decreased statistically significantly across organs in the order of leaves > stems > roots ($p < 0.05$). The $N_{\text{in-SDS}}$ ratio was positively correlated with *LOC107762576*, *LOC107764910*, *LOC107788402*, *LOC107804312*, and *LOC107819268* ($p < 0.05$).

In the alanine, aspartate, and glutamate metabolism pathways (Fig. 9B), N application negatively correlated with *LOC107792671* and *novel.22,893* ($p < 0.05$), and positively correlated with other genes ($p < 0.05$), while cultivar Hongda displayed higher expression of *LOC107810797* and *novel.22,893* compared to K326 ($p < 0.05$). Gene expression at 75 DAT was statistically significantly higher than at 100 DAT ($p < 0.05$), and the *N*w ratio showed positive correlations with *LOC107766022*, *LOC107790669*, *LOC107802035*, *LOC107830560*, and *novel.10,978* ($p < 0.05$).

In the glycine, serine, and threonine metabolism pathways (Fig. 9C), N application statistically significantly suppressed gene expression ($p < 0.05$), with cultivar K326 showing higher expression of *LOC107764643*, *LOC107765918*, and *LOC107811392* compared to Hongda ($p < 0.05$). At 100 DAT, expression of *LOC107764643*, *LOC107781010*, *LOC107783010*, and *LOC107811392* increased statistically significantly ($p < 0.05$), while expression decreased across organs in the order of leaves > stems > roots ($p < 0.05$). Additionally, *LOC107765918*, *LOC107803058*, *LOC107811392*, and *LOC107827351* correlated statistically significantly with *N*s accumulation ($p < 0.05$).

Discussion

Nitrogen (N) is an essential element for plant physiological activities and exists in four distinct morphologies: sodium dodecyl sulfate soluble (N_{S}), water soluble N (N_{W}), sodium dodecyl sulfate insoluble N ($N_{\text{in-SDS}}$), and non-protein N (N_{NP}), each contributing uniquely to specific physiological functions [5]. However, the precise molecular mechanisms governing their distribution remain largely unexplored. Given the functional similarities between these N morphologies and various amino

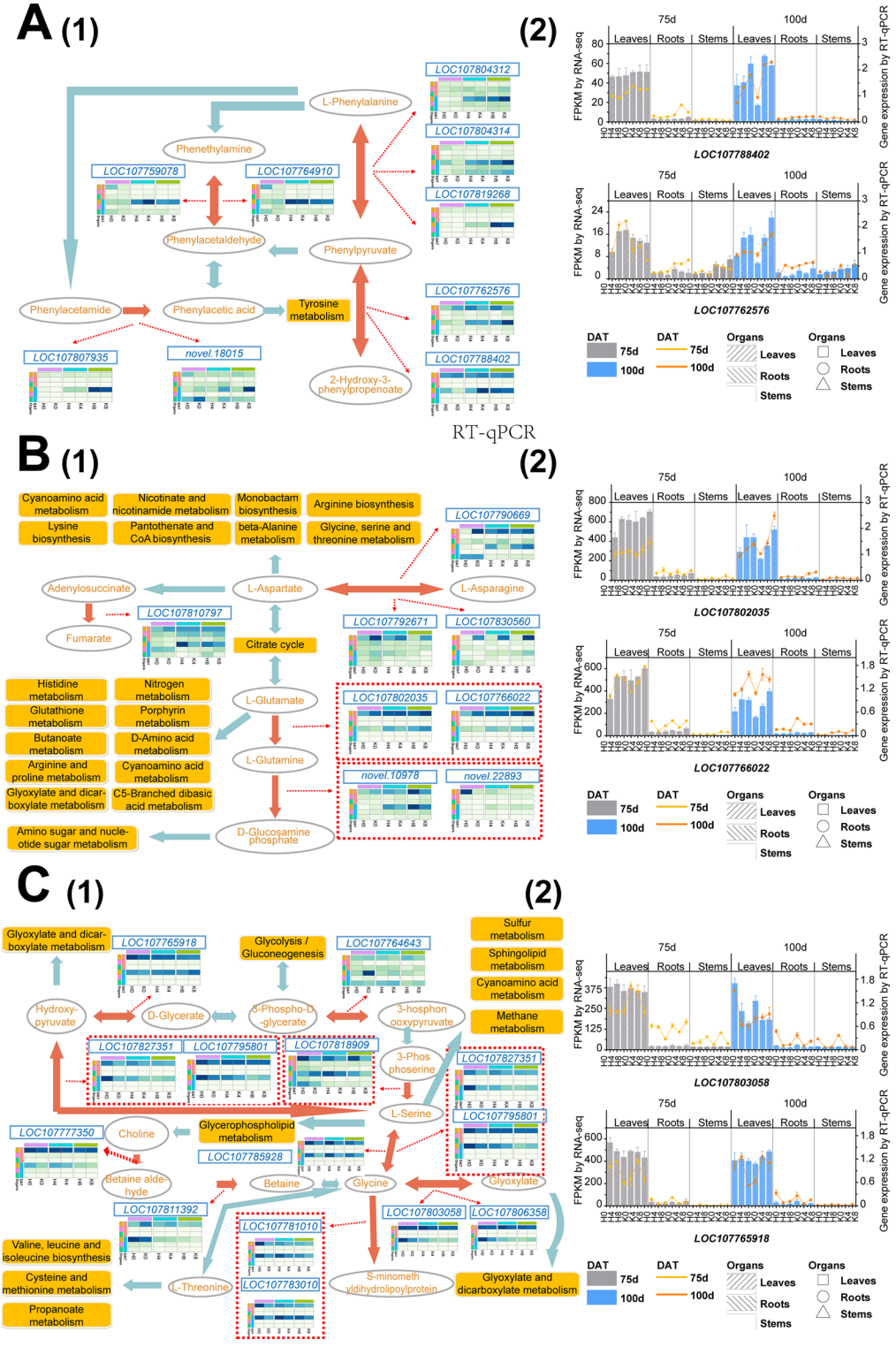

Fig. 8 The amino acid pathway is visualized alongside a heatmap illustrating the expression patterns of related genes in leaves, stems, and roots between the Hongda and K326 cultivars at 75 and 100 days after transplanting under different nitrogen conditions. The bar and line charts present the RT-qPCR results. Panels (**A**) to (**C**) depict the phenylalanine metabolism pathway; the alanine, aspartate, and glutamate metabolism pathways; and the glycine, serine, and threonine metabolism pathways, respectively. Here, H0, H4, and H8 denote the Hongda cultivar under 0 g, 4 g, and 8 g pure nitrogen conditions, respectively, while K0, K4, and K8 represent the K326 cultivar under each nitrogen condition

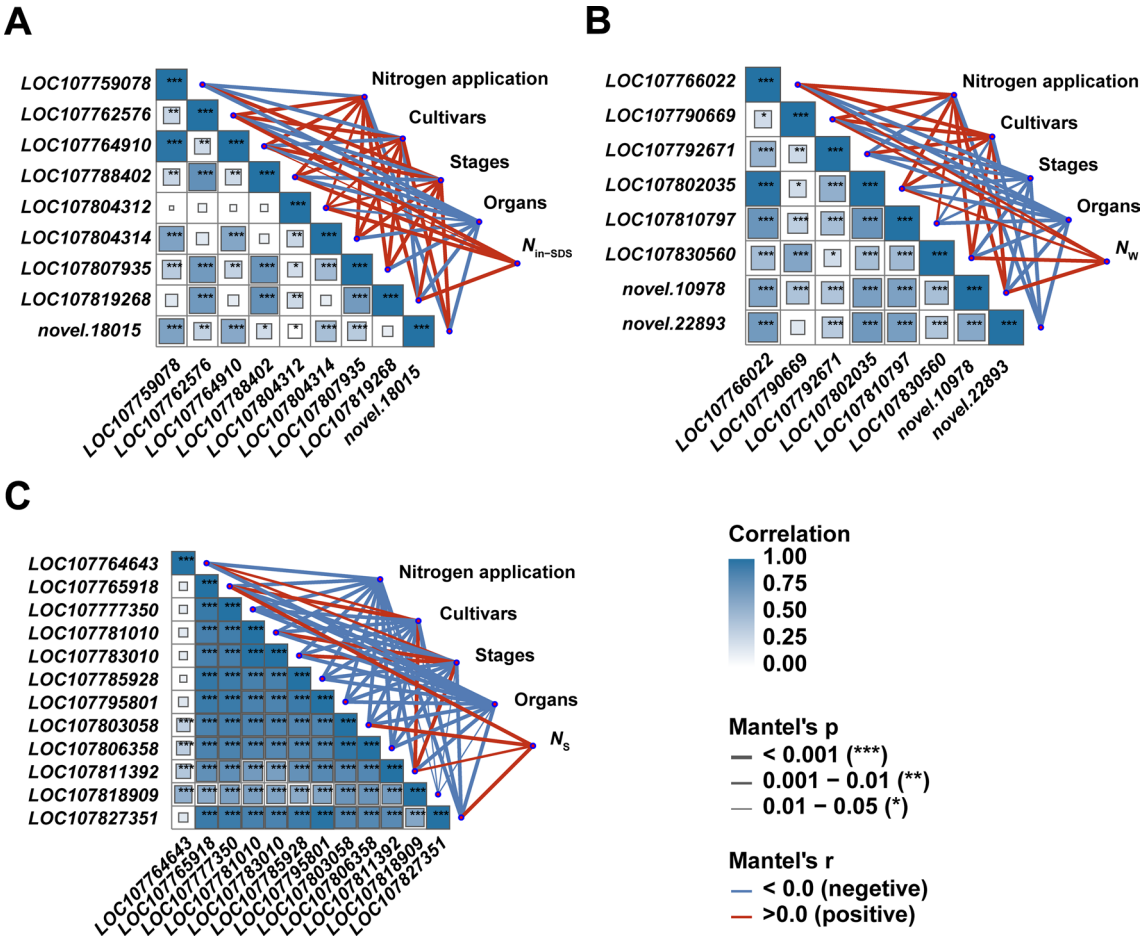

Fig. 9 Mantel test analysis reveals correlations between selected genes in each pathway and various factors, including nitrogen applications, cultivars, stages, organs, and the ratio of corresponding nitrogen morphologies. Panels (**A**) to (**C**) illustrate the phenylalanine metabolism pathway (ko00360), the alanine, aspartate, and glutamate metabolism pathway (ko00250), and the glycine, serine, and threonine metabolism pathways (ko00260), respectively. For calculation purposes, 75 DAT was designated as 1, and 100 DAT was designated as 2, based on plant growth progression; leaves, stems, and roots were labeled as 1, 2, and 3, respectively, reflecting increasing lignification. Hongda and K326 are represented as 1 and 2, respectively. In the visualization, the red lines denote positive relationships, while the blue lines indicate negative relationships. Here, the area and color of each square correspond to the *p* and r values in the correlation analysis: larger squares and darker colors indicate higher r values and *p* values, respectively. Asterisks (*) denote statistical significance levels: * denotes $p < 0.05$, ** denotes $p < 0.01$, and *** denotes $p < 0.001$. Here, $N_{in\text{-}SDS}$ represents sodium dodecyl sulfate insoluble nitrogen, N_S represents sodium dodecyl sulfate soluble nitrogen, N_W represents water soluble nitrogen and N_{NP} present non-protein nitrogen

acid (AA), we hypothesized that N distribution is intricately regulated by genes involved in AA biosynthesis pathways. Distinct AA pathways may modulate N morphologies distribution across different environmental conditions, growth stages, and cultivars, thereby influencing diverse physiological processes. To elucidate these mechanisms, we conducted an in-depth analysis of AA metabolic pathways, aiming to optimize N utilization, improve crop productivity, and promote agricultural sustainability. Our investigation revealed statistically significant differences in N morphologies distribution and biomass accumulation under varying N applications, growth stages, organs, and cultivars. Transcriptome analysis identified notable variations in N metabolism and AA biosynthesis pathways, suggesting their potential roles in regulating N distribution [49]. To enhance the robustness of our findings, we employed F-tests to disentangle the direct effects of N applications, growth stages, cultivars, and organs, enabling precise assessment of individual factor contributions while minimizing confounding effects [44]. Additionally, weighted gene co-expression network analysis (WGCNA) categorized transcriptome data into 16 modules, with the brown, green, and magenta modules positively associated with $N_{in\text{-}SDS}$, N_W, and N_S ratios, respectively. By focusing on gene co-expression patterns, WGCNA reduced the impact of multifactorial interference, facilitating the identification of key molecular mechanisms underlying N distribution. Together, these approaches provide a comprehensive framework for understanding N metabolism in plants [46].

The hub genes within the brown module that were markedly related to $N_{\text{in-SDS}}$ were classified in the phenylalanine metabolism pathway (ko00360). Phenylalanine is a critical precursor in lignin synthesis, first converted into trans-cinnamic acid by phenylalanine ammonia-lyase. Additionally, phenylalanine can contribute to lignin production through aromatic AA deaminases, such as tyrosine ammonia-lyase. The function of phenylalanine in lignin synthesis is essential for enhancing plant growth, quality, and stress resistance by reinforcing cell walls and supporting the plant's structural integrity [50, 51]. Notably, phenylalanine shares similarities with $N_{\text{in-SDS}}$, which is recognized as a morphology of structural N in plants, thereby supporting plant growth [3, 5, 52]. This suggests that the distribution of $N_{\text{in-SDS}}$ may be influenced by genes involved in the phenylalanine metabolism pathway, especially *LOC107762576* (hub gene), *LOC107788402*(hub gene), *LOC107764910*, *LOC107804312*, and *LOC107819268*. Our Mantel analysis further suggested that N application promoted the expression of these genes, further benefiting the interconversion of L-phenylalanine, phenylpyruvate, and 2-hydroxy-3-phenylpropenoate, which are all crucial for lignin biosynthesis [53]. These results align closely with the findings of previous research indicating that N application benefits the regulation of gene expression in the lignin synthesis pathway, ultimately promoting cell wall structure and properties [54, 55]. The green module, associated with the *N*w ratio crucial for plant respiration, contains hub genes linked to the metabolism pathways of alanine, aspartate, and glutamate (ko00250). These AA are essential for the citrate cycle and energy production. Glutamate is transaminated into both aspartic acid and alanine, which are integral to respiration. Aspartic acid provides key intermediates for the citric acid cycle, while alanine, through transamination, forms pyruvate, which is subsequently converted into acetyl-CoA, a vital substrate for ATP synthesis [5, 56–59]. This indicates that both are related to respiration, and the distribution of *N*w can be expected to be regulated by the alanine, aspartate, and glutamate metabolism pathways. Moreover, through the Mantel analysis, we determined that the ratio of *N*w was significantly positively related to *LOC107766022* (hub gene), *LOC107802035* (hub gene), *LOC107790669*, *LOC107830560*, and *novel.10,978* in the pathway, which exhibited relatively high expression levels under relatively high N application, at relatively early growth stages, and in the K326 cultivar. These factors indeed influence the interconversion of metabolites participating in the citrate cycle and respiration. Similarly, reports suggest that N fertilizer enhances the citrate cycle, promoting metabolic activity and plant growth [60]. Second, stronger respiration stages contribute to faster N and biomass accumulation than weaker respiration stages [61, 62], as observed in our research between 75 days after transplanting (DAT) and 100 DAT. Differences in biomass and N accumulation between cultivars may result from variations in gene expression determined by cultivar characteristics [63]. Ultimately, genes involved in the alanine, aspartate, and glutamate metabolism pathways influenced by N applications, growth stages, and cultivar characteristics could further shape *N*w distribution and plant respiration.

The ratio of N_S was closely associated with photosynthesis, particularly electron transfer and light-harvesting functions [5, 64], which had a statistically significant positive correlation with the magenta module. The hub genes in this module are classified into the glycine, serine, and threonine metabolism pathways (ko00260), which play essential roles in optimizing photosynthetic efficiency and light harvesting. Specifically, serine and threonine are involved in the phosphorylation of the light-harvesting system of photosystem II [65–67]. This phosphorylation process enhances the recycling of photosystem II, ensuring that photosynthesis can continue efficiently across various environmental conditions, particularly when light intensity fluctuates [68, 69]. This adaptive capacity is critical for plant survival and growth in competitive environments [70–72]. As hub genes, *LOC107803058* regulates the interconversion of glycine and glyoxylate, controlling photorespiratory N flux, while *LOC107765918* facilitates the conversion of hydroxypyruvate to D-glycerate, linking photorespiration with the carbon recycling process of the Calvin cycle. Their coordinated activity governs the efficiency of photosynthetic carbon recovery. However, the regulation of N distribution (N_S) by these two genes is influenced by external environmental factors in a more complex manner. Additionally, genes such as *LOC107764643*, *LOC107781010*, *LOC107783010*, and *LOC107811392*, involved in glycine, serine, and threonine metabolism pathways, play essential roles in regulating N distribution, participating in processes such as the interconversion of 3-phospho-D-glycerate and 3-phosphonooxypyruvate, the transformation of betaine aldehyde to betaine, the transformation of glycine to S-minomethyldihydrolipoyl protein, and the interconversion of glycine and glyoxylate, all of which are important components of the citrate cycle and respiration. Interestingly, these genes were inhibited by increased N applications, and N applications have been confirmed to lead to damage to the mitochondrial structure of leaves and reduce their number, as well as to disturb leaf N metabolism, eventually restricting electron transport and light harvesting in plants such as maize and Crantz [73, 74]. Ultimately, these results illustrate that the expression of genes involved in the glycine, serine, and threonine metabolism pathways influenced by N

application determines the distribution in N_S and influences plant photosynthesis.

N_{NP} in plants plays a role in storage of N. However, we did not find a specific module regulating the ratio of N_{NP} in plants, possibly because multiple AA pathways may regulate N_{NP} distribution together, which warrants further study. Moreover, the brown, green, and magenta modules were all markedly positively related to biomass and N accumulation, indicating that a greater N distribution in $N_{in\text{-}SDS}$, *N*w, and N_S plants benefits plant growth and N distribution on the basis of stronger structural building, respiration, and photosynthesis abilities [2, 5].

Our findings suggest that the AA biosynthetic pathway plays a pivotal role in regulating N distribution within plants. High expression of genes involved in AA synthesis facilitates N assimilation and directs N toward specific metabolic pathways essential for growth, stress resistance, and energy production. Specifically, genes associated with AA metabolism promote N allocation to structural and metabolic proteins, supporting cell wall synthesis and energy production [50, 51, 56–59, 65–67]. Thus, the high synthesis of AA, driven by the upregulation of specific biosynthetic pathways, directs N toward vital plant processes. This strategic redistribution of N optimizes the plant's metabolic and structural functions, improving growth, stress tolerance, and overall productivity.

While our study provides valuable insights into N distribution mechanisms and their relationship with gene expression in AA metabolism pathways, the lack of metabolomic and proteomic analyses limits the full characterization of the identified hub genes and modules. Future research should address this gap by incorporating metabolomic and proteomic approaches to validate these findings and explore additional regulatory networks [75]. Such efforts are essential to deepen our understanding of N metabolism dynamics in plants, ultimately refining N management strategies [76, 77]. This will not only improve N use efficiency in agriculture but also contribute to more sustainable and effective N application practices, guiding future agricultural practices toward better resource management and environmental sustainability.

Conclusion

This study highlights the pivotal role of amino acid (AA) metabolism in regulating nitrogen (N) distribution across plant organs (leaves, stems, and roots) during different growth stages under varying N application rates. The distribution of N morphologies is influenced by cultivar characteristics, N application rates, growth stages, and environmental conditions, all of which impact plant growth and physiology. Key genes involved in AA metabolism, particularly within the phenylalanine metabolism pathway (ko00360), the alanine, aspartate, and glutamate metabolism pathway (ko00250), and the glycine, serine, and threonine metabolism pathway (ko00260), promote the allocation of specific N morphologies: the phenylalanine metabolism pathway enhances sodium dodecyl sulfate insoluble N ($N_{in\text{-}SDS}$), the alanine, aspartate, and glutamate metabolism pathway favors water soluble N (*N*w), and the glycine, serine, and threonine metabolism pathway facilitates sodium dodecyl sulfate soluble N (N_S). These findings advance our understanding of how AA pathways govern N distribution and offer potential strategies to enhance crop productivity and agricultural sustainability through optimized N management. Future research should integrate multi-omics and real-time physiological assessments to refine nitrogen partitioning mechanisms and enhance nitrogen use efficiency in field conditions.

Abbreviations

N	Nitrogen
N_W	Water soluble nitrogen
N_S	Sodium dodecyl sulfate soluble nitrogen
N_{in-SDS}	Sodium dodecyl sulfate insoluble nitrogen
N_{NP}	Non-protein nitrogen
AA	Amino acid
DAT	Days after transplanting
WGCNA	Weighted gene co-expression network analysis
KEGG	Kyoto Encyclopedia of Genes and Genomes
GO	Gene Ontology
RT-qPCR	quantitative real-time polymerase chain reaction

Supplementary Information

The online version contains supplementary material available at https://doi.org/10.1186/s12870-025-06390-4.

Supplementary Material 1

Author contributions

ZZ conceived and designed the experiments. SL, TJ, DY, LY, XH, and MZ performed the experiments. SL, XP, YY, WZ, and ML collected the data. SL, TJ, and WA analyzed the data and performed the analysis. SL and WA wrote the manuscript. WA and ZZ edited and revised the manuscript. All the authors contributed to the final draft of the manuscript. All authors have read and agreed to the published version of the manuscript.

Funding

This study received financial support from the National Key Research Plan of China (2022YFD1901504) and Development of Dali Specialty Tobacco Leaves for the Exclusive 'Yuxi' High-Quality Cigarette Brand (2020YL03).

Data availability

The original contributions presented in the study are publicly available. This data can be found here: NCBI, PRJNA1116533 and NCBI, PRJNA1118067.

Declarations

Ethics approval and consent to participate

This study does not include human or animal subjects. Consent for publication Not applicable. All experimental studies and experimental materials involved in this research are in full compliance with relevant institutional, national and international guidelines and legislation.

Competing interests

The authors declare no competing interests.

Author details
[1]Yunnan Agricultural University, Kunming, Yunnan 650000, China
[2]Production Department, Yunnan Hongta Group Dali Cigarette Factory, Dali, Yunnan 671000, China
[3]Yunnan Tobacco Monopoly Bureau, Kunming, Yunnan 650000, China
[4]College of Agronomy and Life Sciences, Kunming University, Kunming, Yunnan 650000, China
[5]Academy of Science and Technology, Chuxiong Normal University, Chuxiong, Yunnan 675000, China

Received: 15 November 2024 / Accepted: 12 March 2025
Published online: 27 March 2025

References

1. Xu X, Du X, Wang F, Sha J, Chen Q, Tian G, Zhu Z, Ge S, Jiang Y. Effects of potassium levels on plant growth, accumulation and distribution of carbon, and nitrate metabolism in Apple Dwarf rootstock seedlings. Front Plant Sci 2020, 11.
2. Li S, Ahmed W, Zhang T, Jiang T, Mei F, Shan Q, Yang L, Guo C, Zhao Z. Different morphologies and functional nitrogen accumulation results in the different nitrogen use efficiency of tobacco plants. J Plant Growth Regul. 2023;42(9):5895–908.
3. Takashima T, Hikosaka K, Hirose T. Photosynthesis or persistence: nitrogen allocation in leaves of evergreen and deciduous Quercus species. Plant Cell Environ. 2004;27(8):1047–54.
4. Evans JR, Seemann JR. The allocation of protein nitrogen in the photosynthetic apparatus: costs, consequences, and control. Plant Physiol. 1989;8:183–205.
5. Liu T, Ren T, White PJ, Cong R, Lu J. Storage nitrogen co-ordinates leaf expansion and photosynthetic capacity in winter oilseed rape. J Exp Bot. 2018;69(12):2995–3007.
6. Liu J, Zhang K, Bi J, Yu X, Luo L, Hu L. Mesophyll conductance and N allocation co-explained the variation in photosynthesis in two Canola genotypes under contrasting nitrogen supply. Front Plant Sci. 2023;14:1171331.
7. Qiang B, Zhou W, Zhong X, Fu C, Cao L, Zhang Y, Jin X. Effect of nitrogen application levels on photosynthetic nitrogen distribution and use efficiency in soybean seedling leaves. J Plant Physiol. 2023;287:154051.
8. Haque MA, Haque M. Growth, yield and nitrogen use efficiency of new rice variety under variable nitrogen rates. Am J Plant Sci. 2016;7:612–22.
9. Ren H, Jiang Y, Zhao M, Qi H, Li C. Nitrogen supply regulates vascular bundle structure and matter transport characteristics of spring maize under high plant density. Front Plant Sci. 2020;11:602739.
10. Distelfeld A, Avni R, Fischer AM. Senescence, nutrient remobilization, and yield in wheat and barley. J Exp Bot. 2014;65(14):3783–98.
11. Havé M, Marmagne A, Chardon F, Masclaux-Daubresse C. Nitrogen remobilization during leaf senescence: lessons from Arabidopsis to crops. J Exp Bot. 2017;68(10):2513–29.
12. Kong X, Zhao G. Increasing yield through wheat cultivar mixture that optimizes functional traits within the canopy. Eur J Agron. 2023;151:126977.
13. Song X, Song B, Huo J, Liu H, Adil MF, Jia Q, Wu W, Kuerban A, Wang Y, Huang W. Effect of Boron deficiency on the photosynthetic performance of sugar beet cultivars with contrasting Boron efficiencies. Front Plant Sci 2023, 13.
14. Hildebrandt TM, Nunes Nesi A, Araújo WL, Braun HP. Amino acid catabolism in plants. Mol Plant. 2015;8(11):1563–79.
15. Maeda H, Dudareva N. The Shikimate pathway and aromatic amino acid biosynthesis in plants. Annu Rev Plant Biol. 2012;63:73–105.
16. Li D, Xia K, Zhang H, Li Z, Xie X, Zhou H, Zhai N, Xu G. Silencing of PDC-E1β genes affects Chloroplast development and amino acid metabolism in tobacco. Ind Crops Prod. 2025;225:120488.
17. Zimmermann SE, Benstein RM, Flores-Tornero M, Blau S, Anoman AD, Rosa-Téllez S, Gerlich SC, Salem MA, Alseekh S, Kopriva S, et al. The phosphorylated pathway of Serine biosynthesis links plant growth with nitrogen metabolism. Plant Physiol. 2021;186(3):1487–506.
18. Zhu G, Xiao H, Guo Q, Zhang Z, Zhao J, Yang D. Effects of cadmium stress on growth and amino acid metabolism in two compositae plants. Ecotoxicol Environ Saf. 2018;158:300–8.
19. Shim JS, Jeong HI, Bang SW, Jung SE, Kim G, Kim YS, Redillas M, Oh SJ, Seo JS, Kim JK. DROUGHT-INDUCED BRANCHED-CHAIN AMINO ACID AMINOTRANSFERASE enhances drought tolerance in rice. Plant Physiol. 2023;191(2):1435–47.
20. Lewis RS, Parker RG, Danehower DA, Andres K, Jack AM, Whitley DS, Bush LP. Impact of alleles at the yellow burley (Yb) loci and nitrogen fertilization rate on nitrogen utilization efficiency and tobacco-Specific Nitrosamine (TSNA) formation in Air-Cured tobacco. J Agric Food Chem. 2012;60(25):6454–61.
21. Di H, Wang R, Ren X, Deng J, Deng X, Bu G. Co-composting of fresh tobacco leaves and soil: an exploration on the utilization of fresh tobacco waste in farmland. Environ Sci Pollut Res. 2022;29(6):8191–204.
22. He W, Liu H, Li Y, Wu Z, Xie Y, Yan X, Wang X, Miao Q, Chen T, Rahman S-u, et al. Genome-wide characterization of B-box gene family in Artemisia annua L. and its potential role in the regulation of Artemisinin biosynthesis. Ind Crops Prod. 2023;199:116736.
23. Kayani S-I, Shen Q, Rahman S-u, Fu X, Li Y, Wang C, Hassani D, Tang K. Transcriptional regulation of flavonoid biosynthesis in Artemisia annua by AaYABBY5. Hortic Res. 2021;8:257.
24. Li S, Jiang T, Ahmed W, Yang Y, Yang L, Zhang T, Mei F, Alharbi SA, Shan Q, Guo C et al. Deciphering the impact of nitrogen morphologies distribution on nitrogen and biomass accumulation in tobacco plants. Front Plant Sci 2024, 15.
25. Gan Q, Glantz SA. Relationship between the Chinese tobacco industry and academic institutions in China. Tob Control. 2011;20(1):12–9.
26. Song R, Tan Y, Ahmed W, Zhou G, Zhao Z. Unraveling the expression of differentially expressed proteins and enzymatic activity in response to phytophthora nicotianae across different flue-cured tobacco cultivars. BMC Microbiol. 2022;22(1):112.
27. Yang Y, Ye C, Zhang W, Zhu X, Li H, Yang D, Ahmed W, Zhao Z. Elucidating the impact of Biochar with different carbon/nitrogen ratios on soil biochemical properties and rhizosphere bacterial communities of flue-cured tobacco plants. Front Plant Sci. 2023;14:1250669.
28. Yang Y, Ahmed W, Ye C, Yang L, Wu L, Dai Z, Khan KA, Hu X, Zhu X, Zhao Z. Exploring the effect of different application rates of Biochar on the accumulation of nutrients and growth of flue-cured tobacco (Nicotiana tabacum). Front Plant Sci. 2024;15:1225031.
29. Luo X, Keenan TF, Chen JM, Croft H, Colin Prentice I, Smith NG, Walker AP, Wang H, Wang R, Xu C, et al. Global variation in the fraction of leaf nitrogen allocated to photosynthesis. Nat Commun. 2021;12(1):4866.
30. Li P, Tan X, Liu R, Rahman FU, Jiang J, Sun L, Fan X, Liu J, Liu C, Zhang Y. QTL detection and candidate gene analysis of grape white rot resistance by interspecific grape (Vitis vinifera L. × vitis Davidii Foex.) crossing. Hortic Res. 2023;10(5):uhad063.
31. Ahmad N, Wang X, Zhang X, Li G, Zhao C, Zhao S. Integrated transcriptome and co-expression analysis identified a putative miRNA64-CYP82D27 module regulating oleanane-type saponins biosynthesis in asparagus officinalis. Ind Crops Prod. 2025;226:120637.
32. Ren H, Yang W, Jing W, Shahid MO, Liu Y, Qiu X, Choisy P, Xu T, Ma N, Gao J, et al. Multi-omics analysis reveals key regulatory defense pathways and genes involved in salt tolerance of Rose plants. Hortic Res. 2024;11(5):uhae068.
33. Ahmad N, Hou L, Ma J, Zhou X, Xia H, Wang M, Leal-Bertioli S, Zhao S, Tian R, Pan J, et al. Bulk RNA-Seq analysis reveals differentially expressed genes associated with lateral branch angle in peanut. Genes. 2022;13(5):841.
34. Chen J, Wang J, Wang R, Xian B, Ren C, Liu Q, Wu Q, Pei J. Integrated metabolomics and transcriptome analysis on flavonoid biosynthesis in safflower (Carthamus tinctorius L.) under MeJA treatment. BMC Plant Biol. 2020;20(1):353.
35. Gong Z, Yang C, Dai W, Miao S, Liu Y, Jiao Z, Li B, Xie W, Zhao W, Han X et al. Annexin A1 exerts analgesic effect in a mouse model of medication overuse headache. *iScience* 2023, 26(11).
36. Liu L, Shi B, Li J, Wen J, Zhou L, He Y. Assessing environmental suitability of ligusticum Chuanxiong based on ecological analyses with chemical and molecular verification. Heliyon 2023, 9(3).
37. Kanehisa M, Goto S. KEGG: Kyoto encyclopedia of genes and genomes. Nucleic Acids Res. 2000;28(1):27–30.
38. Pomaznoy M, Ha B, Peters B. GOnet: a tool for interactive gene ontology analysis. BMC Bioinformatics. 2018;19:1–8.
39. Li M, Zhao L-m, Li S-l, Li J, Gao B, Wang F-f, Wang S-p, Hu X-h, Cao J. Wang G-y: differentially expressed LncRNAs and mRNAs identified by NGS analysis in colorectal cancer patients. Cancer Med. 2018;7(9):4650–64.
40. Rahman FU, Zhang Y, Khan IA, Liu R, Sun L, Wu Y, Jiang J, Fan X, Liu C. The promoter analysis of VvPR1 gene: A candidate gene identified through transcriptional profiling of Methyl jasmonate treated grapevine (Vitis vinifera L). Plants. 2022;11(12):1540.
41. Guo CLT, Wong SH, Lau LHS, Lui RNS, Mak JWY, Tang RSY, Yip TCF, Wu WKK, Wong GLH, Chan FKL, et al. Timing of endoscopy for acute upper Gastrointestinal bleeding: a territory-wide cohort study. Gut. 2022;71(8):1544.

42. Wang L, Jing M, Ahmad N, Wang Y, Wang Y, Li J, Li X, Liu W, Wang N, Wang F, et al. Tracing key molecular regulators of lipid biosynthesis in tuber development of Cyperus esculentus using transcriptomics and lipidomics profiling. Plants. 2021;12(10):1492.
43. Rahman FU, Khan IA, Aslam A, Liu R, Sun L, Wu Y, Aslam MM, Khan AU, Li P, Jiang J. Transcriptome analysis reveals pathogenesis-related gene 1 pathway against Salicylic acid treatment in grapevine (Vitis vinifera L). Front Genet. 2022;13:1033288.
44. Occelli L, Zobel L, Stoddard J, Wagner J, Pasmanter N, Querubin J, Renner L, Reynaga R, Winkler P, Sun K et al. Development of a translatable gene augmentation therapy for CNGB1-Retinitis pigmentosa. Mol Ther 2023, 31.
45. Chen P, Zhao M, Tang F, Hu Y, Peng X, Shen S. The effect of plant compartments on the broussonetia papyrifera-associated fungal and bacterial communities. Appl Microbiol Biotechnol. 2020;104(8):3627–41.
46. Wang R, Shu P, Zhang C, Zhang J, Chen Y, Zhang Y, Du K, Xie Y, Li M, Ma T, et al. Integrative analyses of metabolome and genome-wide transcriptome reveal the regulatory network governing flavor formation in Kiwifruit (Actinidia chinensis). New Phytol. 2022;233(1):373–89.
47. Dekel C, Morey R, Hanna J, Laurent LC, Ben-Yosef D, Amir H. Stabilization of hESCs in two distinct substates along the continuum of pluripotency. *iScience* 2022, 25(12).
48. Quilodrán CS, Currat M, Montoya-Burgos JI. Benchmarking the Mantel test and derived methods for testing association between distance matrices. *Molecular Ecology Resources* 2023, 未标注卷号.
49. Zhang Q, Liu M, Ruan J. Integrated transcriptome and metabolic analyses reveals novel insights into free amino acid metabolism in Huangjinya tea cultivar. Front Plant Sci 2017, 8.
50. Perkowski MC, Warpeha KM. Phenylalanine roles in the seed-to-seedling stage: not just an amino acid. Plant Sci. 2019;289:110223.
51. Winkel-Shirley B. Flavonoid biosynthesis. A colorful model for genetics, biochemistry, cell biology, and biotechnology. Plant Physiol. 2001;126(2):485–93.
52. Hikosaka K, Shigeno AJ. The role of Rubisco and cell walls in the interspecific variation in photosynthetic capacity. Oecologia. 2009;160(3):443–51.
53. Xu M, Li H, Luo H, Liu J, Li K, Li Q, Yang N, Xu D. Unveiling the role of β-Glucosidase genes in Bletilla striata's secondary metabolism: A Genome-Wide analysis. Genes. 2024;25(23):13191.
54. Camargo ELO, Nascimento LC, Soler M, Salazar MM, Lepikson-Neto J, Marques WL, Alves A, Teixeira PJPL, Mieczkowski P, Carazzolle MF, et al. Contrasting nitrogen fertilization treatments impact xylem gene expression and secondary cell wall lignification in Eucalyptus. BMC Plant Biol. 2014;14(1):256.
55. Pitre FE, Lafarguette F, Boyle B, Pavy N, Caron S, Dallaire N, Poulin P-L, Ouellet M, Morency M-J, Wiebe N, et al. High nitrogen fertilization and stem leaning have overlapping effects on wood formation in Poplar but invoke largely distinct molecular pathways. Tree Physiol. 2010;30(10):1273–89.
56. Xu C, Fisher R, Wullschleger SD, Wilson CJ, Cai M, McDowell NG. Toward a mechanistic modeling of nitrogen limitation on vegetation dynamics. PLoS ONE. 2012;7(5):e37914.
57. Zou Z, Lin M, Shen P, Guan Y. Alanine-Dependent TCA cycle promotion restores the Zhongshengmycin-Susceptibility in Xanthomonas oryzae. Int J Mol Sci 2023, 24(3).
58. Kirma M, Araújo WL, Fernie AR, Galili G. The multifaceted role of aspartate-family amino acids in plant metabolism. J Exp Bot. 2012;63(14):4995–5001.
59. Xiaochuang C, Meiyan W, Chunquan Z, Chu Z, Junhua Z, Lianfeng Z, Lianghuan W, Qianyu J. Glutamate dehydrogenase mediated amino acid metabolism after ammonium uptake enhances rice growth under aeration condition. Plant Cell Rep. 2020;39(3):363–79.
60. Xin W, Zhang L, Zhang W, Gao J, Yi J, Zhen X, Du M, Zhao Y, Chen L. An integrated analysis of the rice transcriptome and metabolome reveals root growth regulation mechanisms in response to nitrogen availability. Int J Mol Sci 2019, 20(23).
61. Hansen JW, Pedersen A-GU, Berntsen J, Rønbøg IS, Hansen LS, Lomstein BA. Photosynthesis, respiration, and nitrogen uptake by different compartments of a Zostera Marina community. Aquat Bot. 2000;66(4):281–95.
62. Khan NM, Imran M, Ashraf M, Arshad H, Awan AR. Oxytetracycline and Ciprofloxacin antibiotics exhibit contrasting effects on soil microflora, nitrogen uptake, growth, and yield of wheat (Triticum aestivum L). J Soil Sci Plant Nutr. 2022;22(3):3788–97.
63. Ustun H, Dogan A, Peker B, Ural C, Cetin M, Ozyigit Y, Erkan M. Determination of the relationship between respiration rate and ethylene production by fruit sizes of different tomato types. J Sci Food Agric. 2023;103(1):176–84.
64. Ali AA, Xu C, Rogers A, Fisher RA, Wullschleger SD, Massoud E, Vrugt JA, Muss JD, McDowell NG, Fisher JB. A global scale mechanistic model of photosynthetic capacity (LUNA V1.0). Geosci Model Dev. 2016;9(2):587–606.
65. Martínez-Carrasco R, Sánchez-Rodriguez J, Pérez P. Changes in chlorophyll fluorescence during the course of photoperiod And in response to drought in casuarina equisetifolia forst. And forst. Photosynthetica. 2002;40(3):363–8.
66. Willig A, Shapiguzov A, Goldschmidt-Clermont M, Rochaix JD. The phosphorylation status of the Chloroplast protein kinase STN7 of Arabidopsis affects its turnover. Plant Physiol. 2011;157(4):2102–7.
67. Trotta A, Suorsa M, Rantala M, Lundin B, Aro EM. Serine and threonine residues of plant STN7 kinase are differentially phosphorylated upon changing light conditions and specifically influence the activity and stability of the kinase. Plant J. 2016;87(5):484–94.
68. Britt RD, Marchiori DA. Photosystem II, poised for O2 formation. Science. 2019;366(6463):305–6.
69. Höhner R, Pribil M, Herbstová M, Lopez LS, Kunz H-H, Li M, Wood M, Svoboda V, Puthiyaveetil S, Leister D et al. Plastocyanin is the long-range electron carrier between photosystem II and photosystem I in plants. *Proceedings of the National Academy of Sciences* 2020, 117(26):15354–15362.
70. Umar AW, Naeem M, Hussain H, Ahmad N, Xu M. Starvation from within: how heavy metals compete with essential nutrients, disrupt metabolism, and impair plant growth. Plant Sci. 2025;353:112412.
71. Li W, Sun J, Zhang X, Ahmad N, Hou L, Zhao C, Pan J, Tian R, Wang X, Zhao S. The mechanisms underlying salt resistance mediated by exogenous application of 24-Epibrassinolide in peanut. Int J Mol Sci. 2022;23(12):6376.
72. Ahmad N, Naeem M, Ali H, Alabbosh KF, Hussain H, Khan I, Siddiqui SA, Khan AA, Iqbal B. From challenges to solutions: the impact of melatonin on abiotic stress synergies in horticultural plants via redox regulation and epigenetic signaling. Sci Hort. 2023;321:112369.
73. Xing H, Zhou W, Wang C, Li L, Li X, Cui N, Hao W, Liu F, Wang Y. Excessive nitrogen application under moderate soil water deficit decreases photosynthesis, respiration, carbon gain and water use efficiency of maize. Plant Physiol Biochem. 2021;166:1065–75.
74. Omondi JO, Lazarovitch N, Rachmilevitch S, Yermiyahu U, Sperling O. High nitrogen availability limits photosynthesis and compromises carbohydrate allocation to storage in roots of manihot esculenta Crantz. Front Plant Sci. 2019;10:1041.
75. Raziq A, Zhang K, Sun W, Ahmad N, Zhao H, Raza MA, Ahmed S, Din AMU, Zhao S, Pan J, et al. Transcriptome profiling of MYB-overexpressed Transgenic lines provides crucial molecular insights into anthocyanin and remodel the biosynthesis regulatory network in Nicotiana tabacum. Ind Crops Prod. 2024;213:118374.
76. Ahmad N, Zhang K, Ma J, Yuan M, Zhao S, Wang M, Deng L, Ren L, Gangurde SS, Pan J, et al. Transcriptional networks orchestrating red and Pink testa color in peanut. BMC Plant Biol. 2023;23(1):44.
77. Zhang X, Ahmad N, Zhang Q, Wakeel Umar A, Wang N, Zhao X, Zhou K, Yao N, Liu X. Safflower flavonoid 3′5′hydroxylase promotes Methyl Jasmonate-Induced anthocyanin accumulation in Transgenic plants. Int J Mol Sci. 2023;28(7):3205.

Publisher's note